

Cell motility driven by actin polymerization

Alexander Mogilner^{*}, George Oster[†]

^{*} Department of Mathematics, University of California, Davis, CA 95616, mogilner@ucdmath.ucdavis.edu

[†] Department of Molecular and Cellular Biology, University of California, Berkeley, CA 94720-3112, goster@nature.berkeley.edu

ABSTRACT

Certain kinds of cellular movements are apparently driven by actin polymerization. Examples include the lamellipodia of spreading and migrating embryonic cells, and the bacterium *Listeria monocytogenes*, that propels itself through its host's cytoplasm by constructing behind it a polymerized tail of cross-linked actin filaments. Peskin et al. (1993) formulated a model to explain how a polymerizing filament could rectify the brownian motion of an object so as to produce unidirectional force. Their "brownian ratchet" model assumed that the filament was stiff and that thermal fluctuations affected only the 'load', i.e. the object being pushed. However, under many conditions of biological interest, the thermal fluctuations of the load are insufficient to produce the observed motions. Here we shall show that the thermal motions of the polymerizing filaments can produce a directed force. This 'elastic brownian ratchet' can explain quantitatively the propulsion of *Listeria* and the protrusive mechanics of lamellipodia. The model also explains how the polymerization process nucleates the orthogonal structure of the actin network in lamellipodia.

Introduction

Many cell movements appear to be driven by the polymerization of actin. The most conspicuous example is the lamellipodia of crawling cells. Certain gram-negative pathogenic bacteria, such as *Listeria*, *Shigella*, and *Rickettsia*, move intracellularly by polymerizing a 'comet tail' of crosslinked actin filaments that propel them through their host's cytoplasm (Marchand, et al., 1995; Sanger, et al., 1992; Southwick, et al., 1994).

Submitted to: Biophysical Journal

Running Title: Cell motility driven by actin polymerization

Keywords: Actin polymerization, *Listeria*, bacterial propulsion, lamellipodia, cytoskeleton

Several lines of evidence suggest that these motions may be a physical consequence of polymerization itself. For example, actin polymerization can drive polycationic beads placed on the dorsal surface of lamellipodia (Forscher, et al., 1992). Moreover, the sperm cells of the nematode *Ascaris* crawl via a lamellipodium that appears identical to that of mammalian cells; however, the polymer driving this motile appendage is ‘**major sperm protein**’ (MSP), a protein unrelated to actin (Roberts, et al., 1995). Vesicles derived from sperm membrane will also grow a tail of polymerized MSP and move in a *Listeria*-like fashion. This suggests that the propulsive force generated by polymerizing actin filaments has more to do with the physics of polymerization than to any property peculiar to actin.

Recently, Peskin, et al. formulated a theory for how a growing polymer could exert an axial force (Peskin, et al., 1993). They showed that by adding monomers to its growing tip, a polymer could rectify the free diffusive motions of an object in front of it. This process produced an axial force by employing the free energy of polymerization to render unidirectional the otherwise random thermal fluctuations of the load. Their model assumed that the polymer was infinitely stiff, and so the brownian motion of the load alone created a gap sufficient for monomers to intercalate between the tip and the load. Consequently, this model predicts that velocity will depend on the size of the load through its diffusion coefficient. However, recent experiments have cast doubt on this mechanism of propulsion:

- *Listeria* and *Shigella* move at the same speed despite their very different sizes (Goldberd, et al., 1995).
- The actin network at the leading edge of lamellipodia is organized into an orthogonal network (Small, et al., 1995). This is unexplained by the brownian ratchet model, which treats only collinear filament growth.

To remove these limitations, we have generalized the brownian ratchet model to include the elasticity of the polymer and to relax the collinear structure of growing tips. The principle result of this paper will be an expression for the effective polymerization velocity of a growing filament as a function of the load it is working against and its angle to the load. We use this expression to describe the propulsion of *Listeria* and the protrusion of lamellipodia, and discuss the agreement of our estimates with experimental measurements, as well as predictions of the model.

The force exerted by a single polymerizing filament

In this section we describe the physical model for the thermal fluctuations of a free end of an actin filament. We explicitly take into account undulation (i.e. entropic) forces only (Sackmann, 1996), and ignore the cytoplasmic fluid flow (Grebecki, 1994).

We model a polymerizing actin filament as an elastic rod whose length grows by addition of monomers at the tip at a rate $k_{\text{on}}M$ [s^{-1}] and shortens by losing subunits at a rate k_{off} [s^{-1}], where k_{on} [$\text{s}^{-1}\mu\text{M}^{-1}$] is the polymerization rate and M [μM^{-1}] the local molar concentration of monomers near the growing tip. The values of all the parameters we use are gathered in Tables 1 and 2.

An actin filament can be characterized by its persistence length, λ [μm] which is related to its bending modulus, B , by $B = \lambda k_{\text{b}}T$, where k_{b} is Boltzmann's constant and T the absolute temperature (Janmey, et al., 1994). The data on the numerical value of λ varies between $0.5 \mu\text{m}$ (Kas, et al., 1993) to $15 \mu\text{m}$ (Isambert, et al., 1995) depending on the experimental conditions. We feel that the lower measurements are more realistic for filaments under cellular conditions, and so we shall use the value $\lambda \approx 1 \mu\text{m}$. We focus our attention on the actin filaments that constitute the 'free ends' at the growing surface of a crosslinked actin gel. To make the model tractable, we shall make the following simplifying assumptions:

- The thermal fluctuations of the filaments are planar.
- All filaments impinge on the load at the same angle, θ , and they polymerize with the same angle dependent rate, V .
- The free ends of each filament are the same length, ℓ . That is, the growing region is of constant width, behind which the filaments become crosslinked into a gel.
- We consider only one fluctuation mode, neglecting collective modes of the whole actin network; i.e. we treat the body of the network as a rigid anchor.

The assumed spatio-angular structure of the actin network is shown in Figure 1.

Figure 1. (a) Schematic of a free actin filament tip of length ℓ impinging on a load at an angle θ . A filament tip can add a monomer only by a bending fluctuation of amplitude δ equal to half the diameter of an actin monomer. The polymerization rate is $k_{\text{on}}M - k_{\text{off}}$, where M is the monomer concentration. The actin network behind the last crosslink is regarded as a rigid support.

(b) The mechanical equivalent of (a). The bending elasticity is equivalent to a spring constant, κ , given by equation (2). y is the equilibrium distance of the tip from the load, and x is the deviation of the tip from its equilibrium position.

As the filaments polymerize, their brownian motions impinge on the load (e.g. the bacterial wall, or the cytoplasmic surface of the plasma membrane) exerting a pressure. However, in order to add a monomer to the tip of a free filament end a thermal fluctuation must create a gap sufficient to permit intercalation. For a filament approaching the load perpendicularly, a gap half the size of an actin monomer is necessary to enable a monomer to intercalate between the tip and the

membrane (the actin filament is a double helix so a gap of only $\delta \approx 2.7$ nm is required). For a filament approaching at an angle θ to the load, the required fluctuation amplitude is $\delta \cos(\theta)$. The frequency with which these gaps appear, along with the local concentration of actin monomers, determines whether, and how fast, the gel surface can advance. A freely polymerizing tip advancing at an angle θ would grow at a velocity

$$V_p = \Delta (k_{on}M - k_{off}). \quad (1)$$

where $\Delta = \delta \cos(\theta)$ is the projected size of a monomer onto the direction of protrusion (c.f. Appendix A.1). However, because of the load, the actual velocity of the gel front will be less than V_p .

A filament bends much more easily than it compresses, and so the major mode of thermal motion for a single fiber is a bending undulation. In Appendix B we show that a filament impinging on the load at an angle θ behaves as an effective 1-dimensional spring with an elastic constant given by

$$k(\ell, \theta) = \frac{4 k_B T}{\ell^3 \sin^2(\theta)} \frac{f_0(\ell, \theta)}{\sin^2(\theta)} \quad (2)$$

The statistical motion of a filament tip subject to a harmonic restoring force of the effective spring and a load force can be described by a Fokker-Planck equation. In Appendix C we use the fact that the thermal fluctuations of the filament tips is much faster than the polymerization rate to solve this Fokker-Planck equation using perturbation theory; the result is the following expression for the velocity:

$$V = [k_{on}M \hat{p}(\theta, y_0) - k_{off}] \quad (3)$$

where

$$\hat{p}(\theta, y_0) = \frac{\int_0^\infty \exp\left(-\frac{(x - y_0)^2}{2k_B T}\right) dx}{\int_0^\infty \exp\left(-\frac{(x - y_0)^2}{2k_B T}\right) dx} \quad (4)$$

Equation (3) resembles the expression (1) for a freely polymerizing filament if we interpret $\hat{p}(\theta, y_0)$ as a probability of a gap of sufficient size and duration to permit

intercalation of a monomer¹. The expression for $\hat{p}(\theta, y_0)$ given by (4) depends on the average asymptotic equilibrium distance of the tip from the load, y_0 , which can be found as follows.

The potential energy of the filament free end is $E_y = \frac{1}{2}\kappa(x - y_0)^2$, where x is the instantaneous position of the tip and y_0 its elastic equilibrium position, both relative to the load. In Appendix D we use this potential to derive the average force that a thermally fluctuating filament exerts on the load:

$$f(y_0) = k_B T \frac{\exp\left(-\frac{y_0^2}{2k_B T}\right)}{\int_0^\infty \exp\left(-\frac{(x - y_0)^2}{2k_B T}\right) dx} \quad (5)$$

It is easy to show that $f(y_0)$ is monotonically decreasing. Thus equation (5) can be inverted to give $y_0(f)$ and inserted into (3) and (4) to yield the following load-velocity relationship, which is the principle result of this paper:

$$V = \delta \cos(\theta) [k_{\text{on}} M p(\theta, f) - k_{\text{off}}] \quad (6)$$

Here $p(\theta, f) = \hat{p}(\theta, y_0(f))$ is the steady state probability of a gap of width $\delta \cos(\theta)$ between the filament tip and the force, f . Note that the expression for this probability also depends on the flexibility of the filament tip through the parameters ℓ and λ .

In general, function $p(\theta, f)$ must be computed numerically. The generic shape of the load-velocity relationship, $V(f, \theta)$, is shown in Figure 2. A crucial feature is that the filament growth velocity is not a monotonic function of the angle, but passes through a maximum at a critical filament angle θ_c . The reason is clear: thermal fluctuations may not be able to bend a stiff filament acting normal to the load sufficiently to permit intercalation. Since a filament growing nearly parallel to the load cannot exert an axial thrust, there must be an optimal angle for which the force generated is greatest. Since filaments will grow fastest in this direction, we expect that in a population of growing filaments those oriented near the optimum angle will predominate. This optimal angle depends on the load force, f , and on the

¹ We have assumed that the only barrier to intercalation is geometric. That is, a gap equal to the projected size of a monomer is necessary and sufficient for intercalation.

flexibility of the free end. The tip flexibility depends on its length, ℓ , which depends on the crosslink density of the gel, and on the bending stiffness of the filaments, B (i.e. their thermal wavelength, λ). Generally, the optimal angle is an increasing function of the load force and bending stiffness, and a decreasing function of the free end length: $\theta_c(f, \lambda, \ell)$.

We define the optimum polymerization velocity as $V^*(f) = V(f, \theta_c(f))$. The projection of the solid line onto the V - f plane in Figure 2 would be a graph of this function.

Figure 2: Polymerization velocity V [nm/s] as a function of load, f , [pN], and filament incidence angle, θ , in degrees for fixed length, $\ell = 30$ nm, and persistence length, $\lambda = 1\mu\text{m}$. The critical angle, θ_c for fastest growth depends on the load; the trajectory of θ_c is shown on the $V(f, \theta)$ surface connecting the loci of maximum velocity at each load. At small load forces, the optimal velocity, $V^* = V(\theta_c) \sim 1\mu\text{m/s}$ for a local monomer concentration of $\sim 45\mu\text{M}$. The figure was computed from the load-velocity expressions (4-6). The parameter values employed in the computations are given in Table 1.

Limiting cases

In Appendix E we derive four limiting cases for the optimal velocity V^* , which apply in different regimes of filament length and load. We characterize these regimes by the following three dimensionless parameters:

$$\omega = f\delta/k_B T, \quad \varepsilon = \kappa_0 \delta^2 / 2k_B T, \quad f = \omega / 2\varepsilon = f / \kappa_0 \delta \quad (7)$$

ω is the dimensionless work expended to bend a filament by δ . ε measures the mean elastic energy stored in a filament that has been bent sufficiently to intercalate one monomer. f measures the load force relative to the force required to bend a filament by one intercalation distance, δ . The four cases we consider are shown on the ω - ε plane in Figure 3, and the optimal angles and velocities are summarized in Table 3. Each of these four cases will be used below to describe different kinds of actin-driven motility.

Figure 3. The ε - ω plane delimiting the four asymptotic regions corresponding to small and large load forces and short (stiff) and long (flexible) filaments tabulated in Table 3.

Polymerization driven cell motility

The model for force generation by actin polymerization casts light on certain aspects of cell motility. In this section we shall examine the model's predictions for two types of cell movement: the motion of the pathogenic bacterium *Listeria monocytogenes*, and the protrusion of lamellipodia in crawling embryonic cells.

The motion of *Listeria*

The bacterial pathogen *Listeria monocytogenes* moves through the cytoplasm of infected cells by polymerizing a tail of crosslinked actin filaments whose average orientation is with the plus (fast polymerizing) end pointing towards the bacterial body (Marchand, et al., 1995; Sanger, et al., 1992; Smith, et al., 1995; Southwick, et al., 1994; Southwick, et al., 1996). Actin polymerization is apparently stimulated at the bacterial surface via the membrane protein ActA (Brundage, et al., 1993; Kocks, et al., 1993; Southwick, et al., 1994). The majority of observations suggest that there is a gap between the actin meshwork and cell surface, and so most filaments are not directly attached to the membrane. The situation is depicted schematically in Figure 4a.

Figure 4. (a) *Listeria* is driven by a front of polymerizing actin filaments. The interface between the actin network and the cell surface is shown schematically. The crosslinked actin network terminates near the membrane with free ends which impinge on the bacterium at acute angles \pm measured from the direction of the propulsion. The free ends are modeled by elastic filaments which are free to execute brownian motion. If a thermal fluctuation is large enough and lasts long enough a monomer may intercalate onto the filament end with polymerization and depolymerization rates ($k_{on} M$) and k_{off} , respectively. The elongated filament is now slightly bent away from its mean equilibrium configuration so that its fluctuations exert an average elastic pressure against the membrane. Opposing the motion is a viscous drag force, f .
(b) The computed load-velocity curve for *Listeria* at a monomer concentration of $M = 10\mu M$. Cellular conditions correspond to a load of only about 20 pN, so the load per filament is small compared to the stall load, $f_s \sim 540$ pN for a tail consisting of $N \sim 300$ working filaments. Thus the bacterium is working in the nearly load-independent plateau region of the curve.

Actin filament lengths are probably controlled by the host's capping proteins; the observed average length of filaments in the tail is $\sim 200 - 400$ nm (Tilney, et al., 1992a; Tilney, et al., 1992b). The tail filaments are heavily cross-linked to one another and into the host's actin cytoskeleton, and so the tail is almost stationary in the cytoplasm of the host cell (Theriot, et al., 1992). The angular distribution of the filaments are predominantly parallel to the bacterium's axis (Tilney, et al., 1992a; Tilney, et al., 1992b; Zhukarev, et al., 1995).

The speed of *Listeria* propulsion is quite variable, but is generally of the order $0.1 \mu m/s$, which is roughly equal to the actin polymerization velocity (Theriot, et al., 1992). While a bacterium's velocity may fluctuate irregularly it does not correlate with the density of the tail meshwork, and there is very little correlation of speed with the concentration of β -actinin, though lack of β -actinin prevents the initiation of directed motion (Dold, et al., 1994; Nanavati, et al., 1994).

Listeria frequently move along circular tracks with radii of a few bacterial lengths (Zhukarev, et al., 1995). When the bacterium reaches the host cell membrane, it

thrusts outward, stretching the membrane into the form of filopod-like protuberance; once stalled in the protuberance, the bacterium wriggles as if it were restrained by the host's cell membrane (Tilney, et al., 1989). These induced filopodia are the mechanism of intercellular infection, for when a neighboring cell contacts the bacterium-containing protuberance, it phagocytotically ingests the bacterium.

Peskin et al. (1993) derived an expression for the effective velocity of propulsion of bacterium thermally fluctuating in front of the rigid immobile actin tail. In Appendix A.2 we demonstrate that, because of *Listeria*'s size and the high effective viscosity of the cytoplasm, its diffusion coefficient is too small to permit monomer intercalation at a rate sufficient to account for the observed velocities, which are close to the free polymerization velocity of actin filaments. Moreover, bacteria of different sizes, *Listeria*, *Shigella* and *Rickettsia*, moved with the same rate in PtK2 cells (Theriot, 1995). Indeed, *E. coli* expressing the IcsA protein on the surface (which plays the role of ActA), moves in *Xenopus* egg extracts at rates faster than the smaller sized *Listeria*. Thus the speed of actin driven propulsion in these organisms does not scale inversely with size as one would expect if the diffusion of the bacteria were being rectified by the polymerizing tail.

These facts suggest that the bacterium's velocity may be driven by rectifying the thermal undulations of the free filament ends rather than the bacterium itself. In Appendix A.3 we show that the effective diffusion coefficient of a filament tip, D_f , is much larger than that of the bacterium: $D_f \gg D_b$. Therefore, the diffusive motion of the bacterium can be neglected on the time scale of filament fluctuations. Based on micrographs (Tilney, et al., 1992a; Tilney, et al., 1992b), it is reasonable to assume that the characteristic distance between tail filaments near the cell wall is of the order of 50 nm. The viscous drag force on a bacterium is $F = (k_B T / D_b) V \approx 20$ pN. From this we can estimate the number of 'working' filament tips is $N \sim 300$, and the load force per filament is $f \sim 0.06$ pN. Using the parameter values from Table 1 and assuming $\theta = 10^\circ$ (Zhukarev, et al., 1995), the effective spring constant for a free end is $k \sim 0.16$ pN/nm. Using the dimensionless quantities in equation (7) to determine the relevant regime, we find that $\epsilon \sim 0.04$ and $f \sim 0.15$; this corresponds to Case 1 in Table 3. Thus under cellular conditions, *Listeria*'s motion is almost load-independent because the load per filament is very small. The corresponding optimal angle is small, so that filaments are oriented almost parallel to the bacterium's axis, which accords with the experimental observations (Zhukarev, et al., 1995). From Table 3 we find that the effective polymerization velocity is given approximately by the free polymerization velocity (c.f. Appendix A.1). Assuming a concentration of polymerization-competent actin monomers at the bacterial wall of $M \approx 10 \mu\text{M}$ (Cooper, 1991; Marchand, et al., 1995), we find that the optimum velocity is $V^* = V_p$

0.3 $\mu\text{m/s}$, which is the same order of magnitude of the experimentally measured values.

Since the optimal velocity is close to the free polymerization velocity, the bacterium is moving at a 'top speed', and it cannot increase its speed even if the filament density is increased. That is, the bacterium is operating in the plateau region of the load-velocity curve shown in Figure 4b. Conversely, if the filament density is lowered considerably, the velocity should remain constant as long as the load force per filament does not exceed ~ 0.4 pN. This will happen when the density of the actin meshwork decreases until $N \sim 20 \text{ pN}/0.4 \text{ pN} \sim 50$, and so we predict that at least this many filaments are necessary to sustain the maximal velocity.

Although the velocity does not appear to depend on the crosslinking density, when the density of cross-links decreases drastically, the tail will ultimately solate completely and the velocity must decrease to zero (Dold, et al., 1994). However, the velocity will remain constant so long as the filament and crosslink densities are high enough to keep the tail fairly rigid, but not so high as to make the average length of free ends too short so that they cannot fluctuate sufficiently to permit intercalation. This critical length can be estimated from the expression $\varepsilon \sim 1$ to be approximately 75 nm. Thus, we predict that a decrease in *Listeria* velocity will occur only when the cross-linking density (or the concentration of γ -actinin) more than doubles its in vitro value.

We can estimate the stall force per filament as follows. At large load forces the filaments become almost parallel to the wall, whereupon $\cos(\theta) \approx 1/\omega$ (Case 2, Table 3). Then the average equilibrium distance of the filament's tip from the load is $y_0 \approx f_s/\kappa$ (c.f. Appendix D, equation D.5). But when this distance becomes equal to $\ell \cos(\theta)$, then the filament is bent nearly parallel to the load, and the propulsion force drops to zero. Thus, $\ell \cos(\theta) \approx \ell k_B T / f_s \delta \approx f_s / \kappa \approx [f_s \ell^3 / (4\lambda k_B T)](1 - (k_B T / (f_s \delta))^2)$, and so

$$f_s = \frac{k_B T}{\ell} \sqrt{\ell^2 + 4} \quad (8)$$

Therefore, using the parameters given in Table 1, the stall force per filament is $f_s \sim 1.8$ pN, and for the whole bacterium $f_s \sim 1.8 \text{ pN} \times 300 = 0.54$ nN. This estimate is consistent with the stalling of the bacterium by the plasma membrane tension when it pushes out its filopodia-like protuberance. In this situation the resisting force is about $2 b \sigma \approx 0.1$ nN, where $b \sim 0.5 \mu\text{m}$ is the radius of the bacterium and $\sigma \approx 0.035$ pN/nm is the surface tension of the plasma membrane. Finally, we estimate that *Listeria* should maintain a constant velocity until a resisting load of $\sim 0.4 \text{ pN} \times 300 = 0.12$ nN is applied. Thereafter, its velocity will decrease until the stall load of

approximately 0.54 nN, depending on the number of working filaments in the tail (c.f. Figure 4b).

We can now see why the observed propulsion velocity does not depend on the size of the bacterium. As its size increases, the effective number of 'working' filaments propelling the bacterium increases with its cross-sectional area (i.e. the square of the size), while the viscous resistance increases only in proportion to its size. Therefore, the larger the cell, the smaller is the load force per filament. Thus larger cells move with the same maximal free polymerization velocity as smaller cells. However, we predict that the stall force is greater for larger bacteria.

Finally, Marchand et al. measured the dependence of *Listeria*'s velocity on the monomeric actin concentration, M (Marchand, et al., 1995). They obtained a Michaelis-Menten-like saturating curve: at small M the velocity grows linearly with M ; at larger M the velocity asymptotes to a limiting value. This is consistent with the polymerization ratchet model since, for small M , the velocity is equal to the free polymerization velocity, which is proportional to M . At larger M , the velocity is eventually limited by the drag resistance of the host cytoplasm, so the velocity must eventually saturate. Theoretically, the maximum propulsion velocity is achieved when the viscous resistance becomes equal to the stall force. Thus we predict that, for small M , the velocity will be size independent, but for large M the limiting velocity will be proportional to bacterial size.

Lamellipodial extension

Locomoting cells move by a cycle of protrusion and adhesion of their leading edge, followed by—or accompanied by—retraction of their trailing edge. One of the principle protrusive organelles is the lamellipod, a thin veil-like structure of filamentous actin extending from organelle-rich cell body in the direction of movement (Small, 1994; Theriot, 1994; Theriot, et al., 1991; Trinkaus, 1984). Lamellipodial protrusion is the result of a coordinated activity of cytoskeletal, membrane and adhesive systems. Here we focus our attention on the mechanochemical aspects of force generation driving protrusion.

The lamellipodia of fibroblasts and keratocytes have been particularly well studied. They consist of a broad, flat cytoplasmic sheet about 200 nm thick and 5 - 15 μm wide. The ventral surface of the lamellipod is adherent to the substratum (Oliver, et al., 1995; Oliver, et al., 1994). Fibroblast lamellipodia advance in irregular pulsatile fashion (Lackie, 1986), while keratocytes protrude more smoothly, appearing to glide at $\sim 1 \mu\text{m/s}$ in such a way that the cell's shape remains unchanged (Lee, et al., 1993). The mechanisms of lamellipodial protrusion are similar in both cell types, but differ in certain aspects. For example, fibroblast lamella are punctuated by microspikes, or

small filopodia containing parallel arrays of actin filaments, while keratocytes lack microspikes, but do contain ribs of parallel actin filaments which generally do not protrude beyond the leading edge. The actin filaments comprising the lamellipod are almost straight and extend from the front edge through the length of lamellipodia, with an average length of 4 - 7 μm . The filaments are crosslinked into a nearly orthogonal network (Small, et al., 1995). The density of crosslinks gives an estimate of the average length of the free filament ends at the leading edge of $\ell \sim 30$ nm. All filaments are oriented with their barbed (plus) ends in the direction of protrusion (Small, et al., 1978), which has led to the assumption that actin polymerization takes place in a narrow region of a few nanometers beneath the plasma membrane, while depolymerization takes place proximally, near the cell center. Figure 5 shows a schematic view of the filaments at the leading edge. We shall treat the lamellipodium as a network of two populations of parallel, crosslinked fibers incident on the cytoplasmic face of the membrane at angles $\pm \theta$.

Figure 5. (a) We model the actin network driving the protrusion of lamellipodia as a bi-orthogonal array of filaments oriented at angles $\pm\theta$ to the membrane normal. The fluctuations of the filament free ends produces an effective pressure on the cytoplasmic face of the plasma membrane. The load force, f , resisting the motion is distributed over a region of the membrane.
 (b) The computed load-velocity curve for a network consisting of 5000 filaments acting on a membrane area of $5 \mu\text{m} \times 0.2 \mu\text{m}$, and at a local monomer concentration of 45 μM .

The situation in lamellipodia is different from *Listeria* because membrane fluctuations can play a decisive role in permitting monomer intercalation effective enough to allow the filaments to polymerize at their maximum rate, oriented normal to the membrane. This would be contrary to the observed orthogonal network comprising the lamellipodium of the keratocyte. The answer, we believe, is that the leading edge of the lamellipodium is not a bare bilayer, but is heavily populated with membrane associated proteins. Actin polymerization is likely stimulated by ActA-like proteins, for when ActA is expressed in mammalian cells, and myristolated to ensure its membrane association, actin is nucleated from the plasma membrane and protrusive activity is stimulated (Friederich, et al., 1995). Indeed, there is ample evidence that many proteins cluster in regions of high membrane curvature (Table 4). These proteins dramatically damp the amplitude of the membrane fluctuations. Since the diffusion coefficients of such proteins are small, the proteins can damp the membrane fluctuations sufficiently to arrest intercalation.

If membrane fluctuations are insufficient to permit polymerization, filament fluctuations in a network of crosslinked fibers can easily accommodate monomer intercalation and drive protrusion. Assuming an average distance between

filaments of ~ 20 nm, the number of filament tips along a strip of leading edge of area $5 \mu\text{m} \times 0.2 \mu\text{m}$ is $N \sim 5000$. In a freely migrating keratocyte, the only load opposing the polymerization is from the membrane tension, $\sigma \approx 0.035$ pN/nm (Cevc, et al., 1987). The corresponding total load force is $F_L \sim 175$ pN, and the load force per filament is $f \sim 0.035$ pN. From equation (7) $\omega \sim 0.02 \ll 1$, and for $\rho_0 \sim 0.6$ pN/nm, $\varepsilon \sim 0.6$. Thus we are in region corresponding to Case 3 from Table 3. Using the parameters from Table 1, we find that the critical angle for fastest growth is $\theta_c \sim 48^\circ$, which is close to the average filament angle observed by Small in lamellipodia of the fish keratocyte (Small, et al., 1995).

At the optimal angle, θ_c , the effective polymerization velocity (c. f. Table 3) is $V^* = k_{\text{on}} M \cos(\theta_c)$. The observed value of $\sim 1 \mu\text{m/s}$ is achieved for a monomer concentration at the leading edge of $M = 45 \mu\text{M}$. While this is higher than the cytoplasmic value of $\sim 10 \mu\text{M}$, the effective concentration of monomer just under the leading membrane edge is probably much higher due to the presence of proteins analogous to ActA in *Listeria*, which recruit polymerization-competent monomers (Friederich, et al., 1995; Kocks, et al., 1993; Southwick, et al., 1995).

The computed load-velocity curve for a lamellipod, using the data in Table 1, is plotted in Figure 4b. Using equation (8) the stall force per filament is $f_s \sim (2 k_B T / \ell)(\lambda / \delta)^{1/2} \sim 5$ pN. The total stall force would then be $5 \text{ pN} \times 5000 \sim 25$ nN. Using a microneedle, Oliver, et al. measured the force required to stop the advancing lamellipodium of a keratocyte as ~ 45 nN which compares favorably with the theoretical value (Friederich, et al., 1995; Kocks, et al., 1993; Oliver, et al., 1995; Oliver, et al., 1994; Southwick, et al., 1995).

We conclude that (i) lamellipodial protrusion is driven by rectified polymerization of the thermally fluctuating actin filaments, and (ii) the orthogonal geometry of the filaments is nucleated by the angular dependence of the protrusion velocity, and is subsequently 'frozen in' by actin crosslinking proteins. We predict that, as the resistance force increases, the filaments of the lamellipodial cytoskeleton will align at angles more parallel to the leading edge of the cell. At the measured stall load, the filaments should be almost parallel to the edge, a conclusion that may be checked experimentally with sufficiently high resolution electron microscopy. We also predict that higher concentrations of actin-binding proteins would produce heavier cross-linking, shorter free ends of the filaments and effectively slower protrusion velocities.

The above analysis depends on the presence of membrane proteins to damp the fluctuations of the bilayer at the leading edge sufficiently to inhibit monomer intercalation. Where the concentration of protein falls sufficiently, the thermal

fluctuations of the membrane will permit intercalation of monomers without the necessity of filament fluctuation. In this situation, the optimal approach angle for filaments is normal to the bilayer ($\theta_c = 0^\circ$). In such regions we expect the actin to crosslink into parallel bundles, rather than an orthogonal network. This may represent the nucleation of microspikes in fibroblasts and filament bundles in keratocytes. This phenomenon is discussed more fully in Mogilner and Oster (submitted).

Finally, we mention that lamellipodial protrusion is often accompanied by a centripetal flow of cytoplasm: particles and ruffles on the dorsal surface of the lamella move towards the perinuclear area. Since this retrograde, or centripetal flow of lamellar substance accompanies cell migration, there must be a counter-flow of material in the lamellipod (Sheetz, 1994; Small, 1994; Stossel, 1993; Theriot, et al., 1991). Fast centripetal flow of up to 100 nm/s is observed in neural growth cone lamellae (Lin, et al., 1995). In fibroblasts the centripetal flow is fast, while in keratocytes it is slow (Sheetz, 1994). An analysis and model for centripetal flow is given in Mogilner and Oster (submitted); this model depends on the velocity formula derived here as a boundary condition.

Discussion

Energetic arguments have long been cited in support of the presumption that actin polymerization can produce an axial force (Cooper, 1991; Hill, et al., 1982). However, thermodynamics can only assert what is energetically possible, but can say nothing about whether a mechanism is mechanically feasible. Here we have analyzed the mechanics of actin polymerization and demonstrated how growing filaments can develop a protrusive pressure.

Previously, Peskin et al. demonstrated that polymerization of a rigid filament could push a load (Peskin, et al., 1993). In their model, the polymerizing filament rectified the thermal motions of the load to produce an axial force. In the analysis presented here we have relaxed the assumption that the filament be rigid. This modification permits us to construct a statistical mechanical model for the motion of the bacteria *Listeria monocytogenes* and the protrusion of lamellipodia. We find that the polymerization ratchet mechanism can account for the major features of these motile phenomena, including the speed and force of the motions and the angular distributions of the filaments.²

² We note, however, that there exist alternative interpretations of the filament geometry in the leading lamella (see discussion in Mogilner and Oster, submitted).

Numerous mechanical phenomena related to bacterial propulsion remain to be elucidated. Among them are the large fluctuations in cell speed (Dold, et al., 1994; Nanavati, et al., 1994) and the threshold thrust for a bacterium to break through the viscoelastic cytoplasmic gel (Tilney, et al., 1992a; Tilney, et al., 1992b; Tilney, et al., 1989). Explanations for these phenomena will require a stochastic treatment for the polymerization velocity. Also, we treated the cytoskeleton of the host cell as an isotropic homogeneous viscous medium; a more complete picture would take into account fluctuations and the dynamic character of the cytoskeleton. Such a treatment may shed light on the phenomenon of persistent circular motions of *Listeria*. We note, however, that circular *Listeria* tracks frequently exhibit denser actin concentrations on the inner radius of the tail (Zhukarev, et al., 1995). Our theory for polymerization-induced force is consistent with this observation, for a denser network implies shorter and hence stiffer free ends, which will generate less propulsive force than the longer ends on the outer radius.

The mean field theory we have employed assumed independent filaments growing with the same speed, subject to the same load force, and exerting the same undulation force on the load. However, another rectification effect may be important. If fluctuations in polymerization rate cause one filament grows faster than its neighbors, then it can 'subsidize' its neighbors' polymerization by propping up the load and creating a gap into which monomers could easily intercalate. This effect would increase our estimates of the effective velocity and load force. Mathematical analysis of this effect involves singular integro-differential equations and will be dealt with in a subsequent publication.

In effect, we have derived boundary conditions at the leading edge of a polymerizing actin network. Other important phenomena associated with cell crawling, such as retrograde flow require force-angle-velocity relationships of the sort obtained here as boundary conditions (Mogilner and Oster, submitted). The polymerization mechanism produces a force normal to the cell boundary. This is sufficient to produce the phenomenon observed in keratocytes that cells move without shape change as if each boundary segment projects along the boundary normal; Lee et al. (1993) called this isometric motion 'graded radial extension'.

Finally, we anticipate that the model developed here will apply to other actin polymerization driven phenomena such as phagocytosis (Swanson, et al., 1995), platelet activation (Winojur, et al., 1995), and the infective protrusions generated by certain viruses, such as vaccinia (Cudmore, et al., 1995). Moreover, the model described here is not restricted to systems driven by actin polymerization. Nematode sperm extend a lamellipodium and crawl by assembling not actin, but an unrelated protein called major sperm protein (MSP) (Roberts, et al., 1995). These lamellipodia

resemble in most aspects those of mammalian cells and we believe that the underlying physics is the same. Vesicles derived from sperm membrane will also grow a tail of polymerized MSP and move in a *Listeria*-like fashion. Roberts measured the dependence of MSP polymerization velocity on the concentration of monomeric MSP. The curve is qualitatively similar to that for *Listeria* (Marchand, et al., 1995). Knowing the polymerization and depolymerization rates of MSP, the size of its monomer, and the bending rigidity and effective length and mesh size of MSP polymers, one can estimate the effective polymerization velocity at various monomeric concentrations and compare it with experimental results.

Acknowledgments

AM was supported by the Program in Mathematics and Molecular Biology, University of California, Berkeley. GO was supported by National Science Foundation Grant DMS 9220719. The authors would like to thank Julie Theriot, Paul Janmey, Casey Cunningham, John Hartwig, Charles Peskin and Tim Elston for valuable comments and criticism.

Notation	Meaning	Value	Source
ℓ	length of free filament end	30 - 150 nm	(Marchand, et al., 1995; Small, et al., 1995; Tilney, et al., 1992a; Tilney, et al., 1992b)
f_s	stall force of keratocyte	45 nN	(Oliver, et al., 1995; Oliver, et al., 1994)
k_{on}	polymerization rate	$11 \text{ s}^{-1}\mu\text{M}^{-1}$	(Pollard, 1986)
M	monomer concentration	10-50 μM	(Cooper, 1991; Marchand, et al., 1995)
k_{off}	depolymerization rate	1 s^{-1}	(Pollard, 1986)
δ	intercalation gap	2.7 nm	(Pollard, 1986)
d	effective radius of actin	4 nm	(Bremer, et al., 1991)
η_c	viscosity of cytoplasm and cytoskeleton	30 poise	(Dembo, 1989; Valberg, et al., 1987)
η	viscosity of fluid component of cytoplasm	0.03 poise	(Dembo, 1989; Fushimi, et al., 1991)
λ	persistence length of actin	1 μm	(Kas, et al., 1993)
a	length of Listeria	6 μm	(Tilney, et al., 1989)
b	radius of Listeria	0.5 μm	(Tilney, et al., 1989)
	membrane surface tension	0.035 pN/nm	(Cevc, et al., 1987)
L	length of lamellipodia	5 μm	(Small, et al., 1995)
θ	filament angle	0 - 45 degrees	(Small, et al., 1995; Tilney, et al., 1992a; Tilney, et al., 1992b; Zhukarev, et al., 1995)

Table 1. Parameter Values.

Symbol	Meaning
B	bending modulus of actin filament = $\lambda k_B T$ [pN-nm ²]
D_b	diffusion coefficient of bacterium [$\mu\text{m}^2/\text{s}$]
D_f	effective diffusion coefficient of filament [$\mu\text{m}^2/\text{s}$]
f	load force [pN]
f_s	stall force [pN]
f	= $\omega/2\varepsilon = f/\kappa_0\delta$ dimensionless load force
$k_B T$	unit of thermal energy = 4.1×10^{-14} dyne-cm = 4.1 pN-nm
N	number of filaments
$p(\theta, f)$	probability of δ -sized gap as a function of the load, f , and angle,
$\hat{p}(\theta, y_0)$	probability of δ -sized gap as a function of the angle, θ , and the equilibrium position of the filament tip, y_0
q	= $V/(\delta k_{on} M)$ dimensionless polymerization velocity
s	ratio of depolymerization and polymerization rates
t	time [s]
V	velocity of filament tip [$\mu\text{m}/\text{s}$]
V^*	= $V(\theta_c)$ maximum polymerization velocity [$\mu\text{m}/\text{s}$]
V_r	= $2D/\delta$ ideal ratchet velocity [$\mu\text{m}/\text{s}$]
V_p	free polymerization velocity [$\mu\text{m}/\text{s}$]
x	position of filament tip [nm]
y_0	equilibrium distance of filament tip measured from the membrane [nm]
	= $\delta \cos(\theta_c)$ = size of sufficient gap to permit intercalation of monomer
ε	= $\kappa_0\delta^2/2k_B T$ = dimensionless bending energy
κ	elastic constant of an actin filament [pN/nm]
σ	membrane tension ≈ 0.035 pN/nm
ω	= $f\delta/k_B T$ dimensionless work to move the load ahead by one monomer

Table 2. Other Notation

Case	Condition	Meaning	Optimal Angle	Optimal Velocity
1	$\epsilon \ll 1$ $f \ll 1$	Long (flexible) filaments, Small load force	$\theta_c \sim 0^\circ$	$V^* \approx \delta k_{on} M$
2	$\epsilon \ll 1$ $\omega \gg 1$	Long (flexible) filaments, Large load force	$\theta_c \sim \cos^{-1} \frac{1}{\omega}$	$V^*(f) = \frac{k_B T}{f} \left(\frac{k_{on} M}{e} - k_{off} \right)$
3	~ 1 or $\epsilon \gg 1$, $\omega \ll 1$	Short (stiff) filaments, Small load force	$\theta_c \sim \tan^{-1} \frac{2\sqrt{\epsilon}}{\omega^{3/2}}$	$V^* \sim \cos(\theta_c) (k_{on} M - k_{off})$
4	$\epsilon \sim 1$ or $\epsilon \gg 1$ $f \gg 1$	Short (stiff) filaments, Large load force	$\theta_c \sim \cos^{-1} \frac{1}{\omega}$	$V^*(f) = \frac{k_B T}{f} \left(\frac{k_{on} M}{e} - k_{off} \right)$

Table 3. Summary of special cases.

PROTEIN	REFERENCE
ActA expressed in mammalian cells at the tips of membrane ruffles.	(Friederich, et al., 1995)
Proteins localized to membrane ruffles	(Ridley, 1994)
rab 8 proteins at the tips of lamellae and ruffles	(Chen, et al., 1993)
Actin nucleation sites at the rims of lamellipodia	(DeBiasio, et al., 1988)
Virus spikes on filopodia	(Mortara, et al., 1989)
Diacylglycerol nucleating actin assembly	(Shariff, et al., 1992)
Coatomers on the rim of the Golgi	(Kreis, 1992)
Receptors clustering in coated pits	(Anderson, et al., 1983)
GPI anchored proteins and calcium pumps in caveolae	(Fujimoto, 1993; Hooper, 1992)

Table 4. Protein localization in regions of high membrane curvature.

Figure Captions

Figure 1. (a) Schematic of a free actin filament tip of length ℓ impinging on a load at an angle θ . A filament tip can add a monomer only by a bending fluctuation of amplitude δ equal to half the diameter of an actin monomer. The polymerization rate is $k_{\text{on}}M - k_{\text{off}}$, where M is the monomer concentration. The actin network behind the last crosslink is regarded as a rigid support.

(b) The mechanical equivalent of (a). The bending elasticity is equivalent to a spring constant, κ , given by equation (2). y is the equilibrium distance of the tip from the load, and x is the deviation of the tip from its equilibrium position.

Figure 2. Polymerization velocity V [nm/s] as a function of load, f , [pN], and filament incidence angle, θ , in degrees for fixed length, $\ell = 30$ nm, and persistence length, $\lambda = 1\mu\text{m}$. The critical angle, θ_c for fastest growth depends on the load; the trajectory of θ_c is shown on the $V(f, \theta)$ surface connecting the loci of maximum velocity at each load. At small load forces, the optimal velocity, $V^* = V(\theta_c) \sim 1\mu\text{m/s}$ for a local monomer concentration of $\sim 45\mu\text{M}$. The figure was computed from the load-velocity expressions (4-6). The parameter values employed in the computations are given in Table 1.

Figure 3. The ε - ω plane delimiting the four asymptotic regions corresponding to small and large load forces and short (stiff) and long (flexible) filaments tabulated in Table 3

Figure 4. (a) *Listeria* is driven by a front of polymerizing actin filaments. The interface between the actin network and the cell surface is shown schematically. The crosslinked actin network terminates near the membrane with free ends which impinge on the bacterium at acute angles $\pm \theta$ measured from the direction of the propulsion. The free ends are modeled by elastic filaments which are free to execute brownian motion. If a thermal fluctuation is large enough and lasts long enough a monomer may intercalate onto the filament end with polymerization and depolymerization rates ($k_{\text{on}}M$) and k_{off} , respectively. The elongated filament is now slightly bent away from its mean equilibrium configuration so that its fluctuations exert an average elastic pressure against the membrane. Opposing the motion is a viscous drag force, f .

(b) The computed load-velocity curve for *Listeria* at a monomer concentration of $M = 10\mu\text{M}$. Cellular conditions correspond to a load of only about 20 pN, so the load per filament is small compared to the stall load, $f_s \sim 540$ pN for a tail consisting of $N \sim 300$ working filaments. Thus the bacterium is working in the nearly load-independent plateau region of the curve.

Figure 5. (a) We model the actin network driving the protrusion of lamellipodia as a bi-orthogonal array of filaments oriented an an angle θ to the membrane normal. The fluctuations of the filament free tips produces an effective pressure on the cytoplasmic face of the plasma membrane. The load force, f , resisting the motion is distributed over a region of the membrane.

(b) The computed load-velocity curve for a network consisting of 5000 filaments acting on a membrane area of $5 \mu\text{m} \times 0.2 \mu\text{m}$, and at a local monomer concentration of $45 \mu\text{M}$.

B.1 Computing the effective spring constant of the filament tip. Bending of filament causes deviation x from the equilibrium position of the tip in the direction normal to the load.

C.1 (a) The jump processes characterizing polymerization and depolymerization (c.f. Peskin, et al., 1993). $P(x, y, t)$ increases at a rate $[k_{\text{on}}MP(x, y + \delta) + k_{\text{off}}P(x, y - \delta)]$ if the gap between the tip and the load is $\geq \delta$, or if $(y + x) > \delta$, or $x > -y + \delta$. At the same time $P(x, y, t)$ decreases with rate $[k_{\text{on}}MP(x, y) + k_{\text{off}}P(x, y)]$. On the other hand, if the gap is too narrow to allow the intercalation of a monomer, or if $x < -y + \delta$, then $P(x, y, t)$ increases at a rate $k_{\text{on}}MP(x, y + \delta)$ and decreases at a rate $k_{\text{off}}P(x, y)$. Thus the domain on which P is defined is $-\infty < y < \infty$ and $-y \leq x < \infty$, as shown in (b).

References

1. Anderson, R., and J. Kaplan. 1983. Receptor-mediated endocytosis. *Modern Cell Biol.* 1:1-52.
2. Berg, H. 1983. *Random Walks in Biology*. Princeton University Press, Princeton, N.J.
3. Bremer, A., R. C. Millonig, R. Sutterlin, A. Engel, T. D. Pollard, and U. Aebi. 1991. The structural basis for the intrinsic disorder of the actin filament: the "lateral slipping" model. *J. Cell Biol.* 115:689-703.
4. Brundage, R. A., G. A. Smith, A. Camilli, J. A. Theriot, and D. A. Portnoy. 1993. Expression and phosphorylation of the *Listeria monocytogenes* ActA protein in mammalian cells. *Proc. Natl. Acad. Sci. USA.* 90:11890-4.
5. Cevc, G., and D. Marsh. 1987. *Phospholipid Bilayers*. Wiley, New York.
6. Chen, Y. T., C. Holcomb, and H.-P. Moore. 1993. Expression and localization of two low molecular weight GTP-binding proteins, Rab8 and Rab10, by epitope tag. *Proc. Natl. Acad. Sci. USA.* 90:6508-12.
7. Cooper, J. A. 1991. The role of actin polymerization in cell motility. *Ann. Rev. Physiol.* 53:585-605.
8. Cudmore, S., P. Cossart, G. Griffiths, and M. Way. 1995. Actin-based motility of vaccinia virus. *Nature.* 378:636-638.
9. DeBiasio, R., L.-L. Wang, G. W. Fisher, and D. L. Taylor. 1988. The dynamic distribution of fluorescent analogues of actin and myosin in protrusions at the leading edge of migrating swiss 3T3 fibroblasts. *J. Cell Biol.* 107:2631-2645.
10. Dembo, M. 1989. Mechanics and Control of the Cytoskeleton in *Amoeba proteus*. *Biophys. J.* 55:1053-1080.
11. Dold, F. G., J. M. Sanger, and J. W. Sanger. 1994. Intact alpha-actinin molecules are needed for both the assembly of actin into the tails and the locomotion of *Listeria monocytogenes* inside infected cells. *Cell Motil. Cytoskeleton* 28:97-107.
12. Forscher, P., C. H. Lin, and C. Thompson. 1992. Inductopodia: A novel form of stimulus-evoked growth cone motility involving site directed actin filament assembly. *Nature.* 357:515-518.
13. Friederich, E., E. Gouin, R. Hellio, C. Kocks, P. Cossart, and D. Louvard. 1995. Targeting of *Listeria monocytogenes* ActA protein to the plasma membrane as a tool to dissect both actin-based cell morphogenesis and ActA function. *Embo. J.* 14:2731-44.

14. Fujimoto, T. 1993. Calcium pump of the plasma membrane is localized in caveolae. *J. Cell Biol.* 120:1147-1157.
15. Fushimi, K., and A. S. Verkman. 1991. Low viscosity in the aqueous domain of cell cytoplasm measured by picosecond polarization microfluorimetry. *J. Cell Biol.* 112:719-25.
16. Goldberd, M., and J. Theriot. 1995. *Shigella flexneri* surface protein IcsA is sufficient to direct actin-based motility. *Proc. Natl. Acad. Sci. USA.* 92:6572 - 6576.
17. Grebecki, A. 1994. Membrane and cytoskeleton flow in motile cells with emphasis on the contribution of free-living amoebae. *Intl. Rev. Cytol.* 148:37-80.
18. Hill, T., and M. Kirschner. 1982. Bioenergetics and kinetics of microtubule and actin filament assembly and disassembly. *Intl. Rev. Cytol.* 78:1-125.
19. Hooper, N. 1992. More than just a membrane anchor. *Curr. Biol.* 2:617-619.
20. Isambert, H., P. Venier, A. Maggs, A. Fattoum, R. Kassab, D. Pantaloni, and M-F. Carlier. 1995. Flexibility of actin filaments derived from thermal fluctuations. Effect of bound nucleotide, phalloidin, and muscle regulatory proteins. *J. Biol. Chem.* 270:11437-44.
21. Janmey, P. A., S. Hvidt, J. Kas, D. Lerche, A. Maggs, E. Sackmann, M. Schliwa, and T.P. Stossel. 1994. The mechanical properties of actin gels. Elastic modulus and filament motions. *J Biol Chem* 269:32503-13.
22. Kas, J., H. Strey, M. Barmann, and E. Sackmann. 1993. Direct measurement of the wave-vector-dependent bending stiffness of freely flickering actin filaments. *Europhys. Lett.* 21:865-870.
23. Kocks, C., R. Hellio, P. Grounon, H. Ohayon, and P. Cossart. 1993. Polarized distribution of *Listeria monocytogenes* surface protein ActA at the site of directional actin assembly. *J. Cell Sci.* 105:699-710.
24. Kreis, T. E. 1992. Regulation of vesicular and tubular membrane traffic of the Golgi complex by coat proteins. *Curr. Opin. Cell Biol.* 4:609-15.
25. Lackie, J. 1986. *Cell Movement and Cell Behaviour.* Allen & Unwin, London.
26. Landau, L., and E. Lifshitz. 1970. *Statistical Physics.* Pergamon Press, London.
27. Lee, J., A. Ishihara, J. A. Theriot, and K. Jacobson. 1993. Principles of locomotion for simple-shaped cells. *Nature.* 362:467-471.
28. Lin, C., and P. Forscher. 1995. Growth cone advance is inversely proportional to retrograde F-actin flow. *Neuron.* 14:763-71.

29. Marchand, J.-B., P. Moreau, A. Paoletti, P. Cossart, M.-F. Carlier, and D. Pantaloni. 1995. Actin-based movement of *Listeria monocytogenes*: Actin assembly results from the local maintenance of uncapped filament barbed ends at the bacterium surface. *J. Cell Biol.* 130:331-343.
30. Mortara, R., and G. Koch. 1989. An association between actin and nucleocapsid polypeptides in isolated murine retroviral particles. *J. Submicro. Cytol. Pathol.* 21:295-306.
31. Nanavati, D., F. T. Ashton, J. M. Sanger, and J. W. Sanger. 1994. Dynamics of actin and alpha-actinin in the tails of *Listeria monocytogenes* in infected Ptk2 Cells. *Cell Motil. Cytoskeleton.* 28:346 - 358.
32. Oliver, T., M. Dembo, and K. Jacobson. 1995. Traction forces in locomoting cells. *Cell Motil. Cytoskeleton.* 31:225-240.
33. Oliver, T., J. Lee, and K. Jacobson. 1994. Forces exerted by locomoting cells. *Semin. Cell Biol.* 5:139-147.
34. O'Malley. 1974. Introduction to singular perturbations. Academic Press, New York.
35. Peskin, C., G. Odell, and G. Oster. 1993. Cellular motions and thermal fluctuations: The Brownian ratchet. *Biophys. J.* 65:316-324.
36. Pollard, T. 1986. Rate constants for the reactions of ATP- and ADP-actin with the ends of actin filaments. *J. Cell Biol.* 103:2747-2754.
37. Ridley, A. 1994. Membrane ruffling and signal transduction. *Bioessays* 16:5-12.
38. Roberts, T., and M. Stewart. 1995. Nematode sperm locomotion. *Curr. Opin. Cell Biol.* 7:13-17.
39. Sackmann, E. 1996. Supported membranes: scientific and practical applications. *Science.* 271:43-48.
40. Sanger, J. M., J. W. Sanger, and F. S. Southwick. 1992. Host cell actin assembly is necessary and likely to provide the propulsive force for the intracellular movement of *Listeria monocytogenes*. *Infection and Immunity* 60:3609-3619.
41. Shariff, A., and E. J. Luna. 1992. Diacylglycerol-stimulated formation of actin nucleation sites at plasma membranes. *Science.* 256:245-47.
42. Sheetz, M. 1994. Cell migration by graded attachment to substrates and contraction. *Semin. Cell Biol.* 5:149-155.
43. Small, J., G. Isenberg, and J. Celis. 1978. Polarity of actin at the leading edge of cultured cells. *Nature.* 272:638-39.

44. Small, J. V. 1994. Lamellipodia architecture: actin filament turnover and the lateral flow of actin filaments during motility. *Semin. Cell Biol.* 5:157-63.
45. Small, J. V., M. Herzog, and K. Anderson. 1995. Actin filament organization in the fish keratocyte lamellipodium. *J. Cell Biol.* 129:1275-1286.
46. Smith, G., D. Portnoy, and J. Theriot. 1995. Asymmetric distribution of the *Listeria monocytogenes* ActA protein is required and sufficient to direct actin-based motility. *Molec. Microbiol.* 17:945-51.
47. Southwick, F., and D. Purich. 1994. Arrest of *Listeria* movement in host cells by a bacterial ActA analogue: implications for actin-based motility. *Proc. Natl. Acad. Sci. USA.* 91:5168-72.
48. Southwick, F., and D. Purich. 1995. Inhibition of *Listeria* locomotion by mosquito oostatic factor, a natural oligoproline peptide uncoupler of profilin action. *Infection and Immunity.* 63:182-9.
49. Southwick, F., and D. Purich. 1996. Intracellular pathogenesis of listeriosis. *New England Jour. Med.* 334:770-6.
50. Stossel, T. 1993. On the crawling of animal cells. *Science.* 260:1086-1094.
51. Swanson, J. A., and S. C. Baer. 1995. Phagocytosis by zippers and triggers. *Trends in Cell Biol.* 5:89-93.
52. Theriot, J. 1995. The cell biology of infection by intracellular bacterial pathogens. *Ann. Rev. Cell Dev. Biol.* 11:213-239.
53. Theriot, J. A. 1994. Actin filament dynamics in cell motility. *Adv. Exp. Med. Biol.* 358:133-45.
54. Theriot, J. A., and T. Mitchison. 1991. Actin microfilament dynamics in locomoting cells. *Nature.* 352:126-131.
55. Theriot, J. A., T. J. Mitchison, L. G. Tilney, and D. A. Portnoy. 1992. The rate of actin-based motility of intracellular *Listeria monocytogenes* equals the rate of actin polymerization. *Nature.* 357:257-60.
56. Tilney, L. G., DeRosier, D.J., Weber, A., and Tilney, M.S. 1992a. How *Listeria* exploits host cell actin to form its own cytoskeleton. II. Nucleation, actin filament polarity, and evidence for a pointed end capper. *J. Cell Biol.* 118:83 - 93.
57. Tilney, L. G., DeRosier, D.J., and Tilney, M.S. 1992b. How *Listeria* exploits host cell actin to form its own cytoskeleton. I. Formation of a tail and how that tail might be involved in movement. *J. Cell. Biol.* 118:71 - 81.

58. Tilney, L. G., and D. A. Portnoy. 1989. Actin filaments and the growth, movement, and spread of the intracellular bacterial parasite, *Listeria monocytogenes*. *J Cell Biol* 109:1597-1608.
59. Trinkaus, J. 1984. *Cells into Organs: Forces that Shape the Embryo*. Prentice Hall, Englewood Cliffs, NJ.
60. Valberg, P. A., and H. A. Feldman. 1987. Magnetic particle motions within living cells. Measurement of cytoplasmic viscosity and motile activity. *Biophys. J.* 52:551-61.
61. Winojur, R., and J. Hartwig. 1995. Mechanism of shape change in chilled human platelets. *Blood.* 85:1736-1804.
62. Zhukarev, V., F. Ashton, J. Sanger, J. Sanger, and H. Shumann. 1995. Organization and structure of actin filament bundles in *Listeria*-infected cells. *Cell Motil. Cytoskeleton.* 30:229-246.

Appendices

A Parameters and estimates

1. THE POLYMERIZATION VELOCITY OF ACTIN. The free polymerization rate of an actin filament is $(k_{\text{on}}M - k_{\text{off}})$, where $k_{\text{on}} \approx 11 \text{ s}^{-1}\mu\text{M}^{-1}$, $k_{\text{off}} \approx 1 \text{ s}^{-1}$ (Pollard, 1986). We take $M \approx 10 \mu\text{M}$ (Cooper, 1991; Marchand, et al., 1995). The length of an acting monomer is approximately 5.4 nm; since the filament is a double helix, each monomer adds $\delta = 2.7 \text{ nm}$ to the filament length. Therefore, the velocity of a freely growing tip is $V_p \approx 0.3 \mu\text{m/s}$.
2. THE DIFFUSION COEFFICIENT FOR LISTERIA. We compute an effective diffusion coefficient for the bacterium from the Einstein relation: $D_b = k_B T / \zeta$, where ζ is the viscous drag coefficient. For a bacterium, we use the expression for an ellipsoid: $\zeta = 2\pi\eta a / (\ln(a/b) - 1/2)$, where a is the length of the cell and b is its radius, and η is the effective viscosity of the cytoplasm (Berg, 1983). Using the dimensions of Listeria, $a \approx 6 \mu\text{m}$, $b \approx 0.5 \mu\text{m}$, and the viscosity of cytoplasm, $\eta \approx 30 \text{ poise}$, we obtain $D_b \approx 7 \times 10^{-5} \mu\text{m}^2/\text{s}$. From this we compute the 'ideal ratchet velocity', $V_r = 2D_b / \delta \approx 0.05 \mu\text{m/s}$ (Peskin, et al., 1993). Thus for Listeria, $V_r \ll V_p$. The viscous drag force on Listeria is $f = \zeta V = 20 \text{ pN}$, where $V = 0.3 \mu\text{m/s}$ is the observed velocity.
3. THE DIFFUSION COEFFICIENT FOR A FILAMENT TIP. An effective diffusion coefficient (normal to the major axis) for the free end of a filament of length ℓ and radius d is $D_f = k_B T / \zeta$, where the friction coefficient, ζ , for a prolate ellipsoid is $\zeta = 4\pi\eta\ell / (\ln(\ell/d) + 1/2)$. Here η is the viscosity of the fluid component of the cytoplasm only, because the free end of a filament is smaller than a mesh size of the actin network. Using the parameter values from Table 1, we obtain $D_f = 4 \mu\text{m}^2/\text{s}$. The corresponding ideal ratchet velocity for Listeria is $V_r = 2D_f / \delta \approx 2500 \mu\text{m/s} \gg V_p$. Thus rectifying the filament fluctuations via polymerization can easily account for the fastest observed velocities of Listeria.

B Geometry and mechanical properties of the filament tip

Consider a single filament crosslinked into a polymer network. Denote by ℓ the length of the 'free end', i.e. the distance from the polymerizing tip to the first crosslink, as shown in . In the absence of thermal fluctuations, the filament would impinge on the load at an angle θ to the load axis. To simplify our analysis we shall assume that the filament fluctuations are planar, and restrict our attention to the case when $\ell/R \ll 1$, where R is the maximum radius of curvature of the fluctuating filament. This is equivalent to assuming that $\ell \ll \lambda$, where λ is the persistence length of an actin filament.

For small deflections, the bent filament has a constant radius of curvature, R . From Fig B.1, we see that the distance of the fluctuating filament from the load is $x = r'\cos(\theta) + r\sin(\theta)$, where $r' = \ell - R\sin(\ell/R) \approx \ell - R(\ell/R - \ell^3/6R^3) \approx \ell^3/6R^2$, and $r = R - R\cos(\ell/R) \approx R - R(1 - \ell^2/2R^2) \approx \ell^2/2R$. Substituting into the equation for x yields $x = \ell/2[(\cos(\theta)/3)(\ell/R)^2 + \sin(\theta)(\ell/R)]$. The condition $\theta \gg \ell/3R$ is equivalent to $\theta \gg (2\ell/9)^{1/2} \approx 5^\circ$. Thus we can neglect the first term, so that $x \approx \sin(\theta)\ell^2/2R$, or $R \approx \sin(\theta)\ell^2/2x$. Then the bending energy of the filament is $E = B\ell/2R^2$, where B is the bending rigidity. This can be expressed in terms of the thermal wavelength, λ , from the relationship $B = \lambda k_B T$ [Doi, 1986 #2494], so that $E \approx [2\lambda k_B T / (\ell^3 \sin^2\theta)] x^2 \equiv \kappa x^2/2$. Thus the effective spring constant of the filament is

$$\kappa(\theta) = \frac{4 k_B T}{\ell^3 \sin^2(\theta)} \quad (\text{B.1})$$

We shall occasionally write this as $\kappa(\theta) = \kappa_0/\sin^2\theta$, where $\kappa_0 \equiv 4\lambda k_B T/\ell^3$.

Figure B.1

C Analysis of the Fokker-Planck equation

In this appendix we will demonstrate that, in the range of parameters characteristic of cell conditions, the load-velocity equation has the generic form given in equation (3). We model a free end of an actin fiber as a linearly elastic filament of rest length $N\delta$, where N is the number of monomers of length $\delta = \delta\cos(\theta)$, and elastic constant k ; the actin filament is an end-to-end concatenation of such monomers. In order to polymerize a monomer onto the tip of the filament, a gap of size δ must be created by the thermal fluctuations of the filament. We place our coordinate system on the moving load with the coordinate axis directed backward towards the cell center. Denote by y the equilibrium position of the filament tip with respect to the load. Because of thermal fluctuations, the location of the tip deviates from y , and we let x be the distance between the current position of the tip and its equilibrium position. Thus the restoring force of the spring is $F(x) = -kx$. The geometry of the situation is shown in Figure C.1

Let $k_{\text{on}}M$ be the rate at which monomers could polymerize onto the tip if it were not occluded by the load. Upon polymerization the equilibrium position of the tip instantly jumps to $(y - \delta)$, while the deviation, x , remains unchanged. Monomers dissociate from the tip at rate k_{off} , upon which the equilibrium position of the tip jumps to $(y + \delta)$, while x remains unchanged.

The configuration of the system can be described by the probability distribution $P(x, y, t)$ which obeys the Fokker-Planck equation

$$\frac{P}{t} = -\frac{\partial P}{\partial x}, \frac{\partial P}{\partial y} + (H_p + H_d) \quad (C.1)$$

where J_x and J_y are the probability fluxes in the directions x and y , respectively, and H_p, H_d are the sources and sinks due to polymerization and depolymerization, respectively.

The flux, J_y , is due to the movement of the equilibrium position of the tip with effective polymerization velocity V in the coordinate system attached to the load. This flux, which does not depend on x , is given by

$$J_y = VP$$

The flux, J_x , is due to thermal fluctuations of the tip. It consists of two terms: (i) thermal motion, which we characterize by a diffusion coefficient, D_f , and (ii) a 'drift' motion driven by the elastic force. We can write the drift velocity as $v = F(x)/\zeta$, where ζ an appropriate drag coefficient which, by the Einstein relationship, can be set to $k_B T/D_f$. Thus this flux is given by

$$J_x = -D_f \frac{\partial P}{\partial x} - \frac{F(x)}{k_B T} P \quad (C.2)$$

The polymerization rate, H_p , is constructed as shown in Figure C.1.

$$H_p = \begin{cases} k_{on}M(P(x, y + \delta) - P(x, y)), & x > -y + \delta \\ k_{on}MP(x, y + \delta), & x < -y + \delta \end{cases} \quad (C.3)$$

$$H_d = \begin{cases} k_{off}(P(x, y - \delta) - P(x, y)), & x > -y + \delta \\ -k_{off}P(x, y), & x < -y + \delta \end{cases} \quad (C.4)$$

Thus the Fokker-Planck equation governing the evolution of $P(x, y, t)$ becomes

$$\begin{aligned} \frac{P}{t} = & D_f \frac{\partial^2 P}{\partial x^2} - V \frac{\partial P}{\partial y} - \frac{D_f}{k_B T} \frac{\partial}{\partial x} (F(x)P) \\ & + \begin{cases} k_{on}M(P(x, y + \delta) - P(x, y)) + k_{off}(P(x, y - \delta) - P(x, y)), & x > -y + \delta \\ k_{on}MP(x, y + \delta) - k_{off}P(x, y), & x < -y + \delta \end{cases} \end{aligned} \quad (C.5)$$

We shall assume that the tip cannot penetrate the load, $J_x(x = -y) = 0$. So the evolution of P is constrained by the reflecting boundary condition at $x = -y$:

$$J_x|_{x=-y} = 0, \text{ or } \frac{dP(x = -y)}{dx} = \frac{F(x)}{k_B T} P(x = -y) = \frac{y}{k_B T} P(x = -y). \quad (C.6)$$

introduce the perturbation expansion: $P = P_0(t, \tau) + \alpha P_1(t, \tau) + \dots$ into equation (C.11), yielding

$$\frac{P_0}{t} + \frac{P_0}{t} + \frac{P_1}{t} + \dots = AP_0 + AP_1 + KP_0 + O(\alpha^2) \quad (C.12)$$

Equating orders up to the first gives

$$\frac{P_0}{t} - AP_0 = 0, O(1) \quad (C.13)$$

$$\frac{P_1}{t} - AP_1 = -\frac{P_0}{t} + KP_0, O(\alpha) \quad (C.14)$$

We can take advantage of the fact that A is a self-adjoint operator (in an appropriate space, with appropriate boundary conditions). Thus it possesses a complete set of orthonormal eigenfunctions, $\{P_0^{(n)}\}$, $n = 0, 1, 2, \dots$, with corresponding real eigenvalues, λ_n : $AP_0^{(n)} = -\lambda_n P_0^{(n)}$; $0 < \lambda_0 < \lambda_1 < \dots$. (The $P_0^{(n)}$ are the functions of x , and both eigenvalues and eigenfunctions are parametrized by the quasi-stationary variable, y .) It is easy to show that $\lambda_0 = 0$ corresponds to the stationary solution, and $P_{0,y}^{(0)}(x) \geq 0$. The general solution to the zero-th order equation (C.13) can be written as

$$P_0(x, y, t) = \sum_{n=0} e^{-\lambda_n(y)t} P_{0,y}^{(n)}(x) G^{(n)}(y, \tau) \quad (C.15)$$

where the functions $G^{(n)}$ are to be found.

The operator A describes the fast thermal fluctuations of the spring. The variable y is changing much more slowly, and can be considered constant on the fast time scale. Thus $P_{0,y}^{(0)}(x)$ describes the stationary distribution of the tip location for each equilibrium position, y . $P_{0,y}^{(n)}$, $n = 1, 2, \dots$ describe the higher order thermal fluctuation modes which decay fast.

The operator B does not depend on t explicitly, so the right hand side of equation (C.14) can be represented in the form:

$$KP_0 - \frac{P_0}{t} = \sum_{n=0} e^{-\lambda_n(y)t} Q_n(x, y, \tau) \quad (C.16)$$

where the functions Q_n can be expressed in terms of the functions $P_{0,y}^{(n)}$ and $G^{(n)}$. In general, equation (C.14) with the right hand side (C.16) will have a solution containing secular terms growing $\sim t$ on the fast time scale, which would invalidate the perturbation expansion for the distribution P . The usual condition for the absence of secular terms is that the right hand side of equation (C.14) is equal to zero:

$$\frac{P_0}{\tau} - BP_0 = 0 \tag{C.17}$$

which describes an evolution of the zeroth approximation, P_0 , on the slow time scale.

In order to find a quasi-stationary solution of equation (C.17) we can neglect the exponentially decaying terms in the expansion (C.15). Thus, we are looking for a quasi-stationary solution of the form $P_0 = p(y,x) g(y, \tau)$. The functions p and g obey the following normalization conditions:

$$\int_{-y}^0 dy g(y, \tau) = 1, \quad \int_{-y}^0 dx p(y,x) = 1$$

Equation (C.17) has the form:

$$p \frac{g}{\tau} = -q \frac{(pg)}{y} + \begin{cases} p(x,y+1)g(y+1) - p(x,y)g(y) + s(p(x,y-1)g(y-1) - p(x,y)g(y)), & x > -y + 1 \\ p(x,y+1)g(y+1) - sp(x,y)g(y), & x < -y + 1 \end{cases} \tag{C.18}$$

Here the function $p(y,x)$ is the solution of the stationary equation:

$$\frac{d^2 p}{dx^2} + x \frac{dp}{dx} = 0 \tag{C.19}$$

Integrating equation (C.19) once, we obtain:

$$\frac{dp}{dx} + xp = 0 \tag{C.20}$$

(The constant of integration is equal to zero because of the zero flux boundary condition at $x = -y$.) The normalized solution of equation (C.20) has the form:

$$p(y, x) = \frac{\exp -\frac{x^2}{2}}{\int_{-y}^{\infty} \exp -\frac{x^2}{2} dx} \quad (C.21)$$

Integrating both sides of equation (C.18) over x we obtain the equation governing slow dynamics of the function g :

$$-\frac{g}{y} = -q \frac{g}{y} + p(y+1)g(y+1) - sg(y) - p(y)g(y) + sg(y-1) \quad (C.22)$$

where the function $p(y)$ is defined as

$$p(y) = \frac{\int_0^{\infty} \exp -\frac{(x-y)^2}{2} dx}{\int_0^{\infty} \exp -\frac{(x-y)^2}{2} dx} \quad (C.23)$$

We are interested in a stationary solution of equation (C.22). An approximate stationary solution of the equation

$$-q \frac{g}{y} + p(y+1)g(y+1) - sg(y) - p(y)g(y) + sg(y-1) = 0 \quad (C.24)$$

can be obtained in the diffusion approximation to this differential-difference equation:

$$-\frac{1}{y} \left[(q+s-p(y))g \right] + \frac{1}{2} \frac{d^2}{dy^2} \left[(s+p(y))g \right] = 0 \quad (C.25)$$

This approximation is valid if $|dp/dy| \ll 1$ (which depends on the filament stiffness and load force). Integrating (C.25) and taking into account the normalization condition on the function g , we obtain the solution of this equation in the form:

$$g = \frac{C}{s+p(y)} \exp \int \frac{2(q+s-p(y))}{s+p(y)} dy \quad (C.26)$$

where C is a normalization constant. This is easy to show from the expression (C.23) that $p(y)$ is monotonically increasing function. Then expression (C.26) has a single maximum at y_0 which is defined approximately by the condition¹:

$$q + s - p(y_0) = 0 \quad (C.27)$$

Thus, if the average equilibrium distance of the polymer tip from the load (defined as the maximum of the probability distribution) is equal to y_0 , then the average effective polymerization velocity can be found from equation (C.27):

$$q = p(y_0) - s, \quad (V/k_{on}M) = p(y_0) - (k_{off}/k_{on}M), \quad V = (k_{on}Mp(y_0) - k_{off}). \quad (C.28)$$

Thus we arrive at the equation for the protrusion velocity (from here on we use dimensional expressions)

$$V = (k_{on}Mp(y_0) - k_{off}) \quad (C.29)$$

where the expression for $p(y_0)$ is given by

$$p(y_0) = \frac{\int_0^{\infty} \exp\left(-\frac{(x - y_0)^2}{2k_B T}\right) dx}{\int_0^{\infty} \exp\left(-\frac{(x - y_0)^2}{2k_B T}\right) dx} \quad (C.30)$$

If we introduce the notation

$$\hat{p}(y_0) = \frac{\int_0^{\infty} \exp\left(-\frac{(x - y_0)^2}{2k_B T}\right) dx}{\int_0^{\infty} \exp\left(-\frac{(x - y_0)^2}{2k_B T}\right) dx} \quad (C.31)$$

the formula for the effective polymerization velocity has the form:

$$V = \cos(\theta) (k_{on}M\hat{p}(y_0) - k_{off}) \quad (C.32)$$

¹ When the model parameters are such that the condition $|dp/dy| \ll 1$ does not hold, and the diffusion approximation is not valid, an approximate analysis of the differential-difference equation (C.24) reveals that the maximum is defined approximately by equation (C.27). This result will be reported elsewhere.

D The force exerted by the fluctuating filament

As in Appendix C, y is the equilibrium position of the filament tip and x is the current position of the tip (this is more convenient here to consider the variable x measured from the load). Then the potential energy of the filament free end is $E_y(x) = \frac{1}{2}\kappa(x - y)^2$, where $(\)$ is given by (B.1). Using this potential we can derive the average force, f , that a thermally fluctuating filament exerts on the load.

The free energy of the tip can be written (Landau and Lifshitz, 1970)

$$G = G_0 - k_B T \ln \int_0^{\infty} e^{-E_y(x)/k_B T} dx \quad (D.1)$$

where $\epsilon \gg \sqrt{k_B T / \kappa}$, and G_0 is the free energy of the tip without the elastic potential. Then the force exerted by the tip on the load is

$$f = \left. \frac{dG}{dZ} \right|_{=0} = \left. \frac{dG_0}{dZ} \right|_{=0} - \frac{k_B T}{Z} \left. \frac{dZ}{dZ} \right|_{=0} \quad (D.2)$$

where the partition function, Z , is given by

$$Z = \int_0^{\infty} e^{-E_y(x)/k_B T} dx \quad (D.3)$$

Now, $\left. \frac{dG_0}{dZ} \right|_{=0} = \frac{k_B T}{Z}$, and so the force is

$$f = k_B T \frac{e^{-E_y(0)/k_B T}}{\int_0^{\infty} e^{-E_y(x)/k_B T} dx} = k_B T \frac{\exp\left(-\frac{y^2}{2k_B T}\right)}{\int_0^{\infty} \exp\left(-\frac{(x-y)^2}{2k_B T}\right) dx} \quad (D.4)$$

It is easy to show that $f(y)$ is one-to-one and monotonically decreasing. There are two limiting cases in which we can approximately invert the function $f(y)$ given by (D.4):

1. the spring force is weak compared to the load, i.e. $\epsilon \ll \omega^2$, or $k_B T \ll f^2$. Then $y < 0$, and $y^2 \gg 2k_B T$, and

$$\int_0^y \exp\left(-\frac{(x-y)^2}{2k_B T}\right) dx = \left(\frac{k_B T}{|y|}\right) \exp\left(-\frac{y^2}{2k_B T}\right),$$

so

$$y = f, \quad f \gg \sqrt{k_B T} \quad (\text{D.5})$$

In this situation, the filament resisting the load is almost always bent and fluctuations are negligible and the force is the same as for a macroscopic spring.

2. The spring force is very strong compared to the load, i.e. $\kappa k_B T \gg f^2$, or $f \gg \sqrt{2 k_B T}$.

Then $y > 0$, and $\kappa y^2 \gg 2 k_B T$, and $\int_0^y \exp\left(-\frac{(x-y)^2}{2k_B T}\right) dx = \sqrt{2 k_B T} \frac{1}{2}$, so

$$y = \sqrt{\frac{k_B T}{2} \ln\left(\frac{k_B T}{f^2}\right)}, f \ll \sqrt{k_B T} \quad (\text{D.6})$$

Thus if the filament is stiff enough, and the load small enough, then the equilibrium position of the tip is far away from the load, and so it exerts a force on the load only rarely when a large thermal fluctuation causes it to hit the load.

E Limiting cases

Long filament, small force

Consider the situation when the elastic energy required for intercalation of a monomer is much smaller than thermal energy, and the work required to bend a filament by one monomer is small, i.e. $\epsilon \ll 1$, $f \ll 1$. The first inequality holds if the length of the filament free end is larger than ~ 75 nm. Then the equilibrium position of the tip, $y_0 \ll \lambda$,

$$\int_0^y \exp\left(-\frac{(x-y_0)^2}{2k_B T}\right) dx = \int_0^y \exp\left(-\frac{(x-y_0)^2}{2k_B T}\right) dx$$

and from (C.31), $p(\theta, f) = \hat{p}(\theta, y_0) \approx 1$; therefore,

$$V = V_p = (k_{on} M - k_{off}). \quad (\text{E.1})$$

In this case, θ_c is small (but not smaller than $\sim 5^\circ$ at which angle the approximation of a harmonic spring becomes invalid), and the optimum polymerization velocity is

$$V^* \approx \delta k_{on} M \quad (\text{E.2})$$

Short or Long filament, large force

When the bending energy is less than thermal energy, and the work to move the load ahead by one monomer distance is much larger than $k_B T$, i.e. $\omega \ll 1$, $\omega \gg 1$, then $f \gg \sqrt{k_B T}$, and from (D.5) we have $y_0 = -f$, and $|y_0| \gg \ell$. The same is true when the filaments are short (shorter than ~ 75 nm, and therefore stiff), but the load force is large, i.e. $\varepsilon \sim 1$ or $\varepsilon \gg 1$ and $f \gg 1$. Then,

$$p(\theta, f) = \hat{p}(\theta, y_0) = \frac{\int_0^{\ell + f/\cos(\theta)} \exp\left(-\frac{(x - y_0)^2}{2k_B T}\right) dx}{\int_0^{\ell + f/\cos(\theta)} \exp\left(-\frac{x^2}{2k_B T}\right) dx} \quad (\text{E } 3)$$

$$\sqrt{\frac{f/\cos(\theta)}{\ell + f/\cos(\theta)}} \exp\left(-\frac{\left(\ell + f/\cos(\theta)\right)^2 - \left(f/\cos(\theta)\right)^2}{2k_B T}\right) \exp(-f \cos(\theta)/k_B T)$$

Then the velocity is

$$V = \cos(\theta) \left[k_{\text{on}} M e^{-f \cos(\theta)/k_B T} - k_{\text{off}} \right] \quad (\text{E } 4)$$

It is easy to check that the maximum of this expression at constant force is reached at

$$\cos(\theta) = \cos^{-1} \frac{1}{\varepsilon} \quad (\text{E } 5)$$

The optimum polymerization velocity is

$$V^*(f) = \frac{k_B T}{f} \left(\frac{k_{\text{on}} M}{e} - k_{\text{off}} \right) \quad (\text{E } 6)$$

where e is the base of the natural logarithms. Thus, at large load force the filaments turn more and more parallel to the load, and the optimum polymerization velocity decreases inversely proportional to the load force.

Short filament, small force

When the length of the filament tip, ℓ , is less than about 75 nm, and the load force is small, i.e. $\varepsilon \sim 1$ or $\varepsilon \gg 1$, $\omega \ll 1$, then $f \ll \sqrt{k_B T}$, and the equilibrium position of the tip is given by expression (D.6). The logarithmic factor in (D.6) can be neglected, and the inequality $|y_0| \ll \ell$ is valid. Then, from (C.31), we have:

$$p(\theta, f) = \hat{p}(\theta, y_0) = \frac{\int_0^{\infty} \exp\left(-\frac{(x - y_0)^2}{2k_B T}\right) dx}{\int_0^{\infty} \exp\left(-\frac{x^2}{2k_B T}\right) dx} \frac{\int_0^{\infty} \exp\left(-\frac{x^2}{2k_B T}\right) dx}{\int_0^{\infty} \exp\left(-\frac{(x + y_0)^2}{2k_B T}\right) dx} \quad (\text{E } 7)$$

There are two cases to consider:

A. When $\theta > \tan^{-1} \frac{2\sqrt{\lambda}}{\rho^{3/2}}$ and $\kappa^2/2k_B T \ll 1$ expression (E 7) is approximately equal to 1, then the velocity is nearly the free polymerization velocity given by equation (1):

$$V = v_{\text{free}} \cos(\theta) (k_{\text{on}} M - k_{\text{off}}) \quad (\text{E } 8)$$

B. When $\theta < \tan^{-1} \frac{2\sqrt{\lambda}}{\rho^{3/2}}$ and $\kappa \Delta^2/2k_B T \gg 1$, expression (E 7) is approximately equal to

$$\frac{[\kappa_B T / \rho] \exp\left(-\frac{\kappa^2}{2k_B T}\right) / \sqrt{\kappa_B T / \rho}}{= (1/\rho) \sqrt{\kappa_B T / \rho} \sin(\theta) \exp\left(-\frac{\rho^2}{2k_B T \sin^2(\theta)}\right)} \quad (\text{E } 9)$$

then the velocity is given by

$$V = k_{\text{on}} M \sqrt{\kappa_B T / \rho} \sin(\theta) e^{-\frac{\rho^2}{2k_B T \sin^2(\theta)}} \quad (\text{E } 10)$$

Expression (E 8) is a decreasing function of the incidence angle, while (E 10) is an increasing function of the angle. They are of the same order when $\theta \sim \tan^{-1} \frac{2\sqrt{\lambda}}{\rho^{3/2}}$.

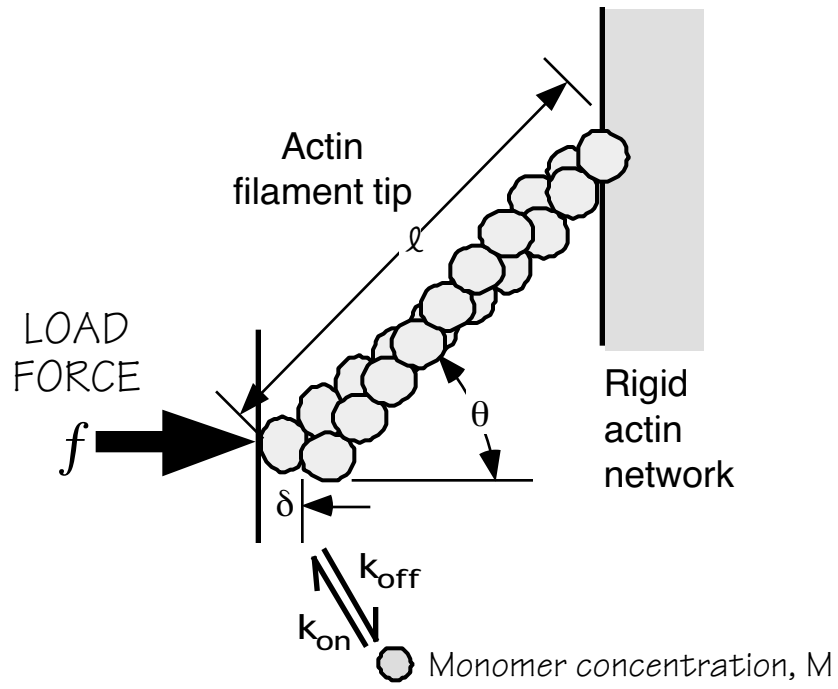
In this case the critical angle for maximal growth rate is

$$\theta_c = \tan^{-1} \frac{2\sqrt{\lambda}}{\rho^{3/2}} \quad (\text{E } 11)$$

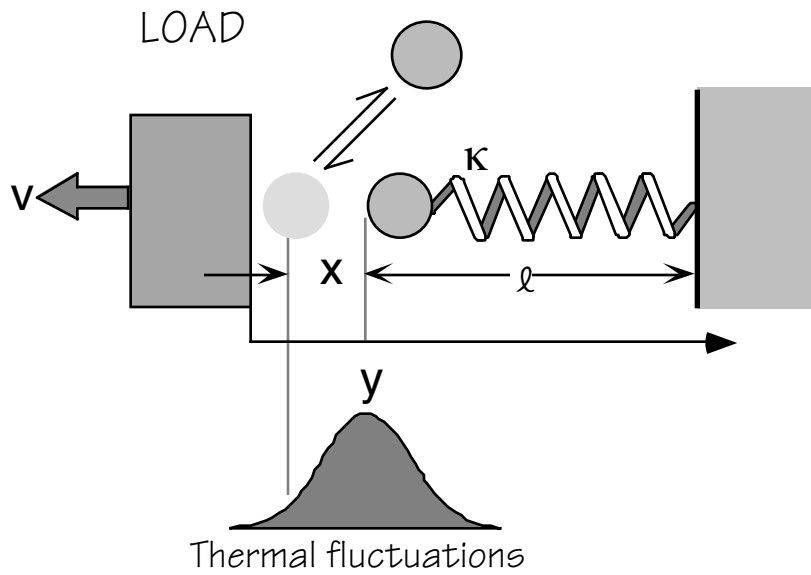
APPENDICES

and the optimum polymerization velocity is

$$V^* = \cos(\theta_c) (k_{\text{on}} M - k_{\text{off}}) \quad (\text{E } 12)$$



(a)



(b)

Figure 1

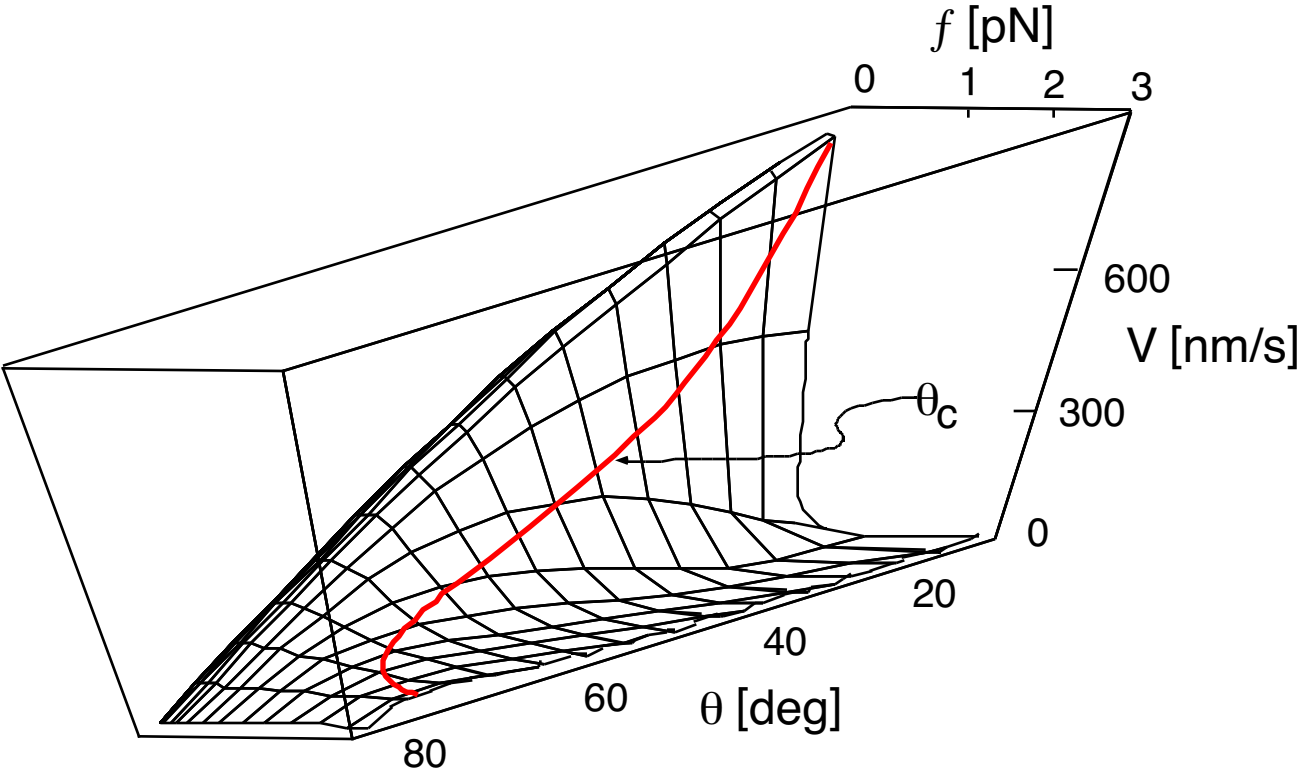


Figure 2

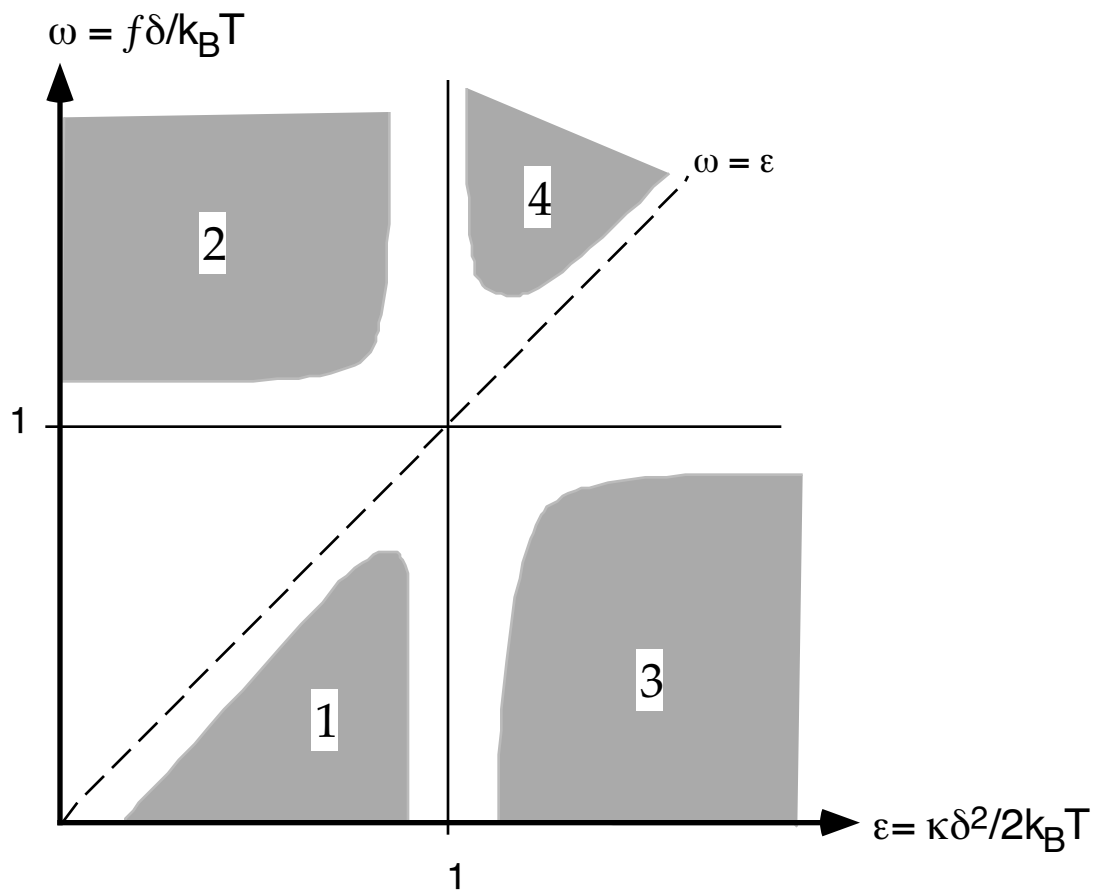


Figure 3

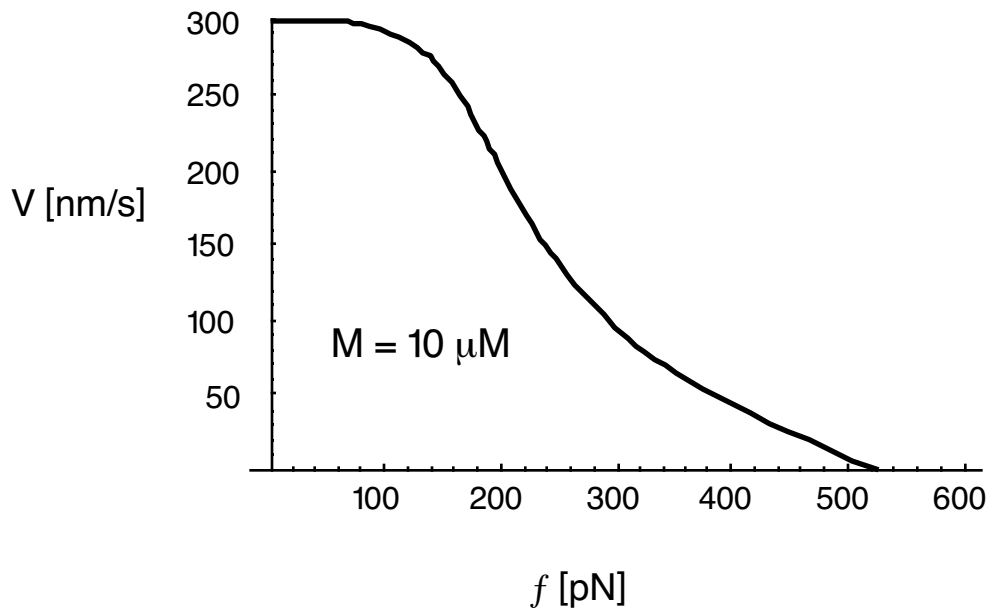
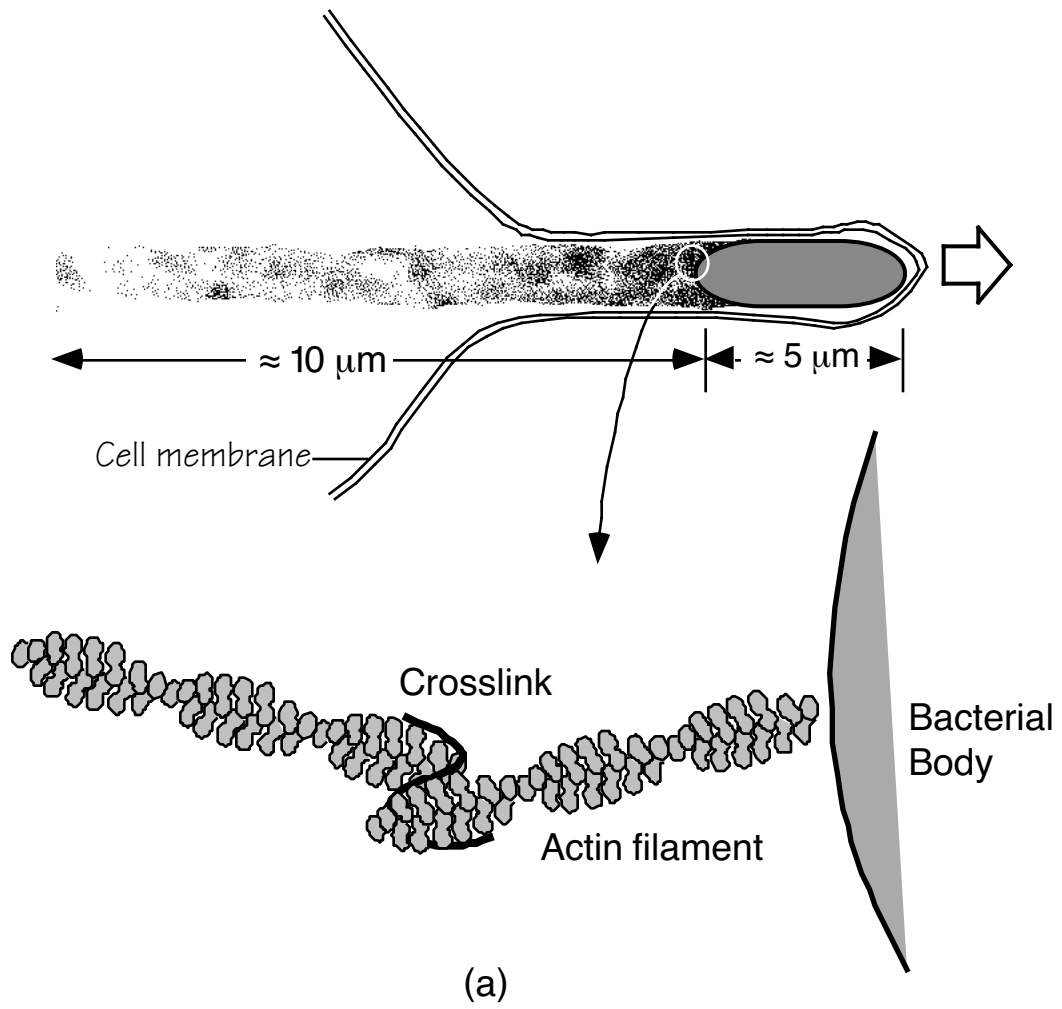


Figure 4

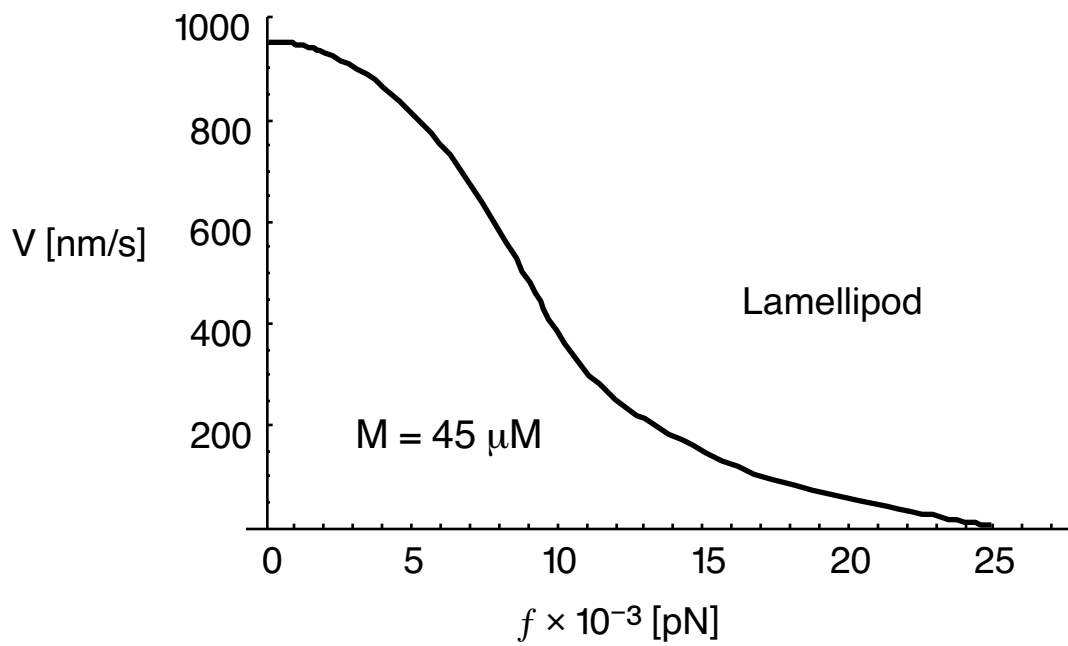
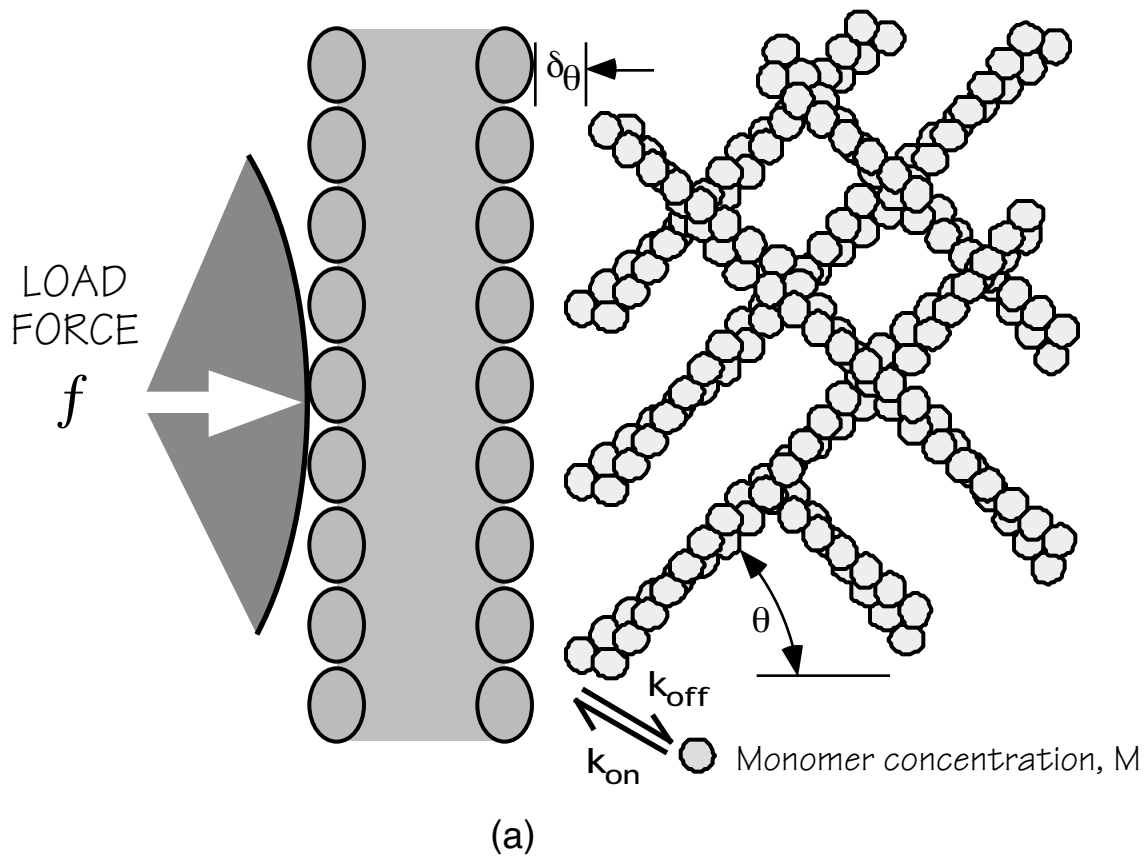


Figure 5

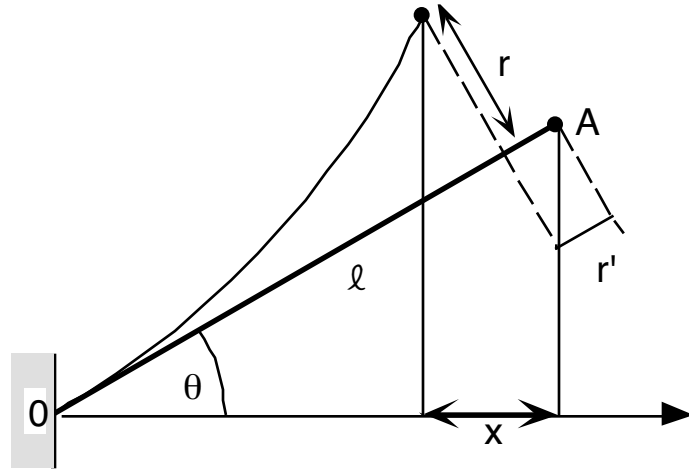
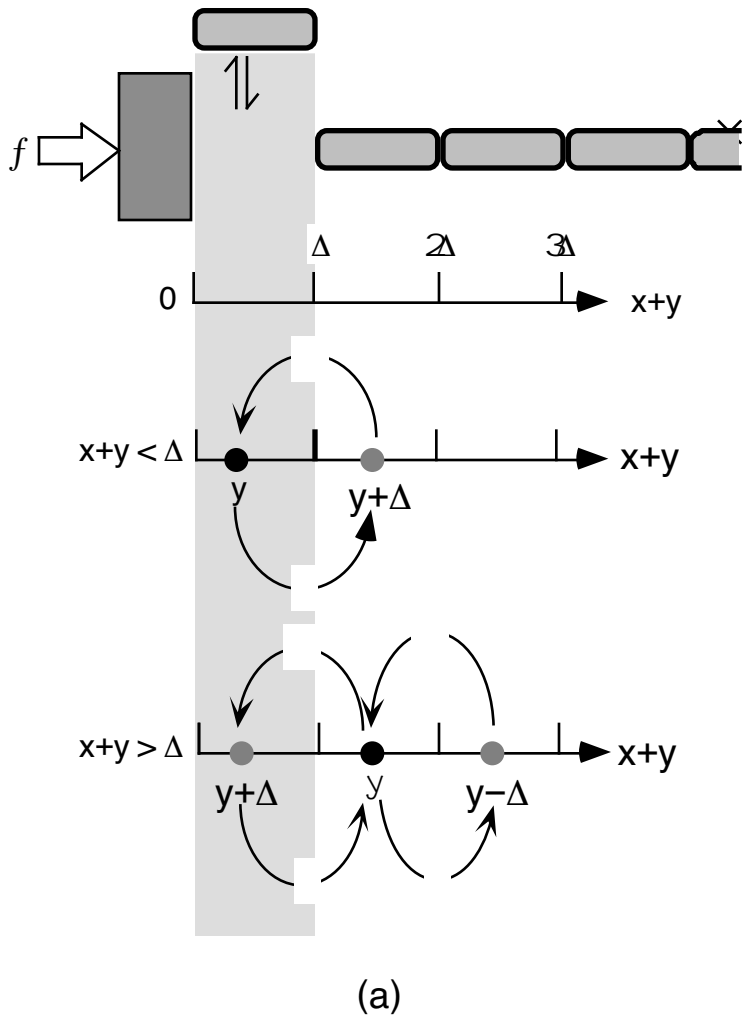
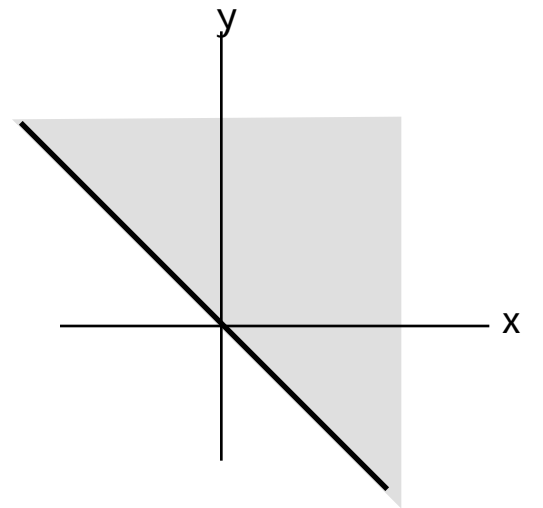


Fig. B1



(a)



(b)

Figure C1